1

Colloidal Molecules and Colloidal Polymers

Etienne Duguet[1], Etienne Ducrot[2], and Serge Ravaine[2]

[1] Université de Bordeaux, Institut de Chimie de la Matière Condensée de Bordeaux (ICMCB, UMR 5026), CNRS, Bordeaux INP, 87 avenue du Dr Albert Schweitzer, Pessac, 33600, France
[2] Université de Bordeaux, Centre de Recherche Paul Pascal (CRPP, UMR 5031), CNRS, 115 avenue du Dr Albert Schweitzer, Pessac, 33600, France

1.1 Introduction

The self-assembly of colloidal objects, inspired by self-organization phenomena observed in nature, is a relevant alternative to chemical synthesis route and top-down fabrication techniques for building increasingly complex structures and materials. It is also an effective tool to understand physicochemical processes that drive self-assembly phenomena as colloidal units are typically three orders of magnitude larger than atoms and molecules and thus can be tracked by optical microscopy techniques [1, 2]. For instance, isotropic spherical particles, often called colloidal atoms (CAs), helped to clarify crystallization and phase transition mechanisms and were observed as they assembled in different phases such as gels, glasses, and several crystal phases [3, 4]. It was shown that interactions between CAs can be tuned by varying the composition of the solvent, by applying external fields and/or concentration gradients, and by modulating the surface chemistry of the particles [5]. Driven by the desire to elaborate colloidal materials possessing new, interesting properties, the field of colloidal self-assembly has made a leap over in the last decades by synthesizing monodisperse particles of various shapes and sizes and by focusing on their assembly through a wide range of interactions [6–8]. In particular, nonspherical colloids stemming from the aggregation of a small number of particles, named "colloidal molecules" (CMs) by van Blaaderen [9], have attracted a lot of attentions these recent years because they are expected to show complex behavior (like low-molecular-weight compounds) dictated not only by the shape of the clusters but also by the variety of the interactions they could generate [10–13]. We have recently proposed a classification of CMs using and extending the well-known formalism of Gillespie derived from the valence shell electron pair repulsion (VSEPR) model (Figure 1.1) [14], which facilitates the reading of this chapter.

Functional Materials from Colloidal Self-assembly, First Edition. Edited by Qingfeng Yan and George Zhao.

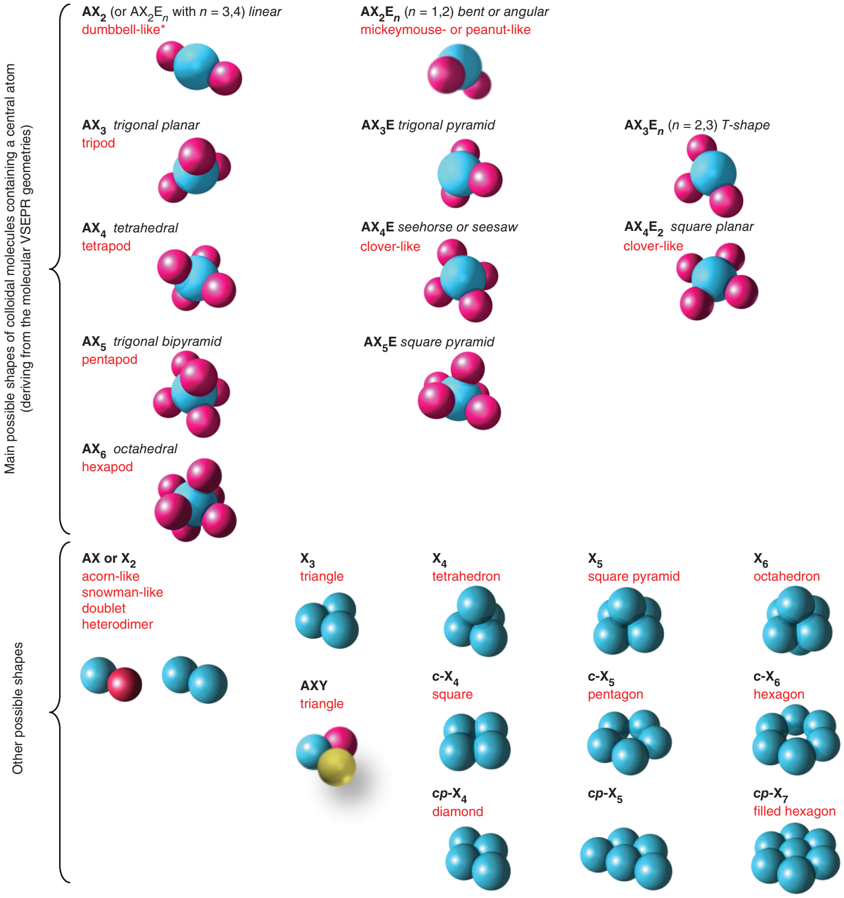

Figure 1.1 Proposition of classification for colloidal molecules based on spheres and mimicking space-filling models of simple molecules. Source: Duguet et al. [14] / with permission from the Royal Society of Chemistry.

The concept of using preformed particles as colloidal monomers has also received recent attention for the formation of one-dimensional (1D) structures, also called “colloidal polymers” (CPs) [15, 16]. A big challenge in the formation of CPs is that it requires strong anisotropic interparticle interactions to minimize side reactions, which is possible to achieve through the development of synthetic methods that allow one to embed anisotropic character to colloidal monomers.

We aim here to highlight and classify the major strategies hitherto reported to fabricate CMs and CPs by self-assembly of preformed particles. We first describe the synthesis pathways to CMs, emphasizing in particular the use of patchy particles as building units. We finally present the different inventive routes that have been developed to create CPs. We restrict the discussion to the synthesis routes and the morphology control, whatever the physical, biological, or chemical properties and potential applications of the CMs and CPs may be.

1.2 Colloidal Molecules: Mimicking Organic and Inorganic Molecules

From the point of view of the synthetic strategy, there exist two main ways to access CMs [14, 17]. The first one concerns essentially AX_nE_m-type CMs and starts from soft or hard preformed CAs decorated by satellite colloids directly generated at their surface, thanks to controlled phase separation or nucleation/growth phenomena, respectively. The second pathway consists in the controlled clustering of preformed CAs through physical routes, chemical routes, or 2D/3D geometrical confinement. The readers who want to embrace the full story have to refer to our previous reviews [14, 17] and/or to read excellent recent reviews written by others and addressing the field from other angles [10–12, 18–25]. In the present chapter, we propose to focus our description of the work in the literature on this second strategy, which relates to the general assembly process.

1.2.1 Clustering of Isotropic Colloids

The following pathways use isotropic spherical CAs, i.e. particles, which surface chemistry and topology are not patterned, meaning they are not spontaneously able to establish interactions in specific directions with other particles.

1.2.1.1 Clustering Assisted by External Fields

These strategies are usually implemented with microparticles on solid surfaces under optical microscope and generate essentially quasi-planar CMs. The strength of the used fields shall also be tuned to overcome the gravity and surface adhesion forces. In this context, Wu and coworkers have reported that applying external alternating current (AC) electric fields is an efficient and simple way to generate anisotropic dipolar and dielectrophoretic interactions between negatively charged polystyrene (PS) microparticles [26]. The morphology of the as-obtained CMs may be quite complex and varied by changing the field frequency via different assembly pathways that resemble chemical reactions of real molecules. Grzybowski and colleagues have shown that magnetic field microgradients established in a paramagnetic fluid can be used as virtual molds to serve as templates for the production of a variety of CMs, including A_4, A_5, A_6, AX_2, AX_3, and AX_4 types (Figure 1.2) [27]. The assembly of CAs into CMs has also been driven by a magneto-acoustic method by Yellen and coworkers. The CM morphology can be tuned by varying the magnetic and acoustic fields that allow to control the interparticle interactions and the local density of particles by attracting them to the pressure nodes of the standing wave, respectively [28]. Although attractive for their ease of use and high morphology yield, these synthesis routes assisted by external fields suffer from very low production yield and sometimes from lacking fixation strategy for making the CM structure permanent (after suppression of the fields). However Grzybowski and colleagues have shown that this last issue may be solved by attaching the CMs to the substrate with carbamide bonds, making them permanent by silica deposition before their release into a liquid by sonication [27].

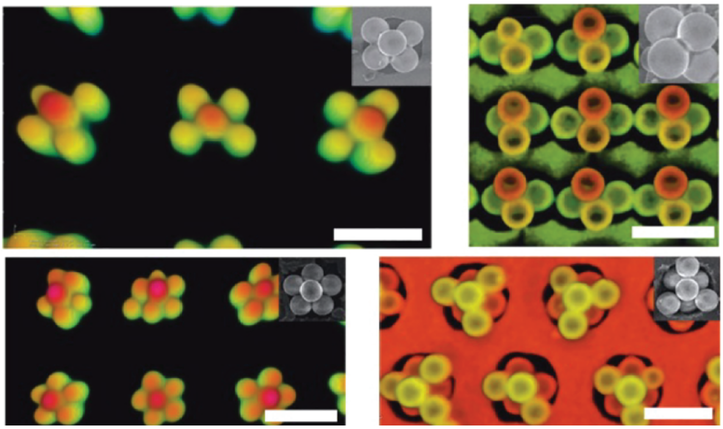

Figure 1.2 CMs of diamagnetic particles with X_4, X_5, X_6, and X_7 geometries obtained under magnetic field microgradients established in a paramagnetic fluid. Scale bars: 2 μm. Source: Demirörs et al. [27] / with permission of Springer Nature.

1.2.1.2 Clustering Assisted by Geometrical Confinement

The patterning of 2D substrates with hydrophilic patches [29] or traps [30] allows the controlled sequential deposition of microparticles, resulting in the creation of a wide library of CMs, including 3D chiral objects. Nevertheless, the production yields remain low. Another strategy consists in the adsorption of particles onto emulsion droplets used as 3D templates, i.e. taking advantage of the Pickering effect, followed by their aggregation through the droplet phase evaporation. This is the pioneering pathway opened by Manoharan and colleagues [31] which has inspired van Blaaderen to develop the concept of CMs [9]. When during evaporation the CAs touch another on the surface of the droplets, removing more liquid causes the droplet to deform and generates capillary forces that collapse the CAs into a CM [31]. The structures of these CMs include familiar polyhedra, e.g. X_4 and X_6, and ones that are more unusual. The selection of a unique packing arises almost entirely from geometrical constraints [32]. Nevertheless, the size polydispersity of the initial emulsion droplet leads to complex mixtures of different CMs that can be finally sorted by density gradient centrifugation. Using narrow droplet size distribution through ultrasonication, Witteman and coworkers have obtained similar CMs from 150-nm particles (Figure 1.3) [33]. Later, Monte Carlo simulations have allowed a full description of the dynamics correlated to experiments [34]. Crassous and colleagues have recently investigated again this route with thermosensitive particles, e.g. poly(*N*-isopropylacrylamide) (PNIPAM) microgels, and achieved CMs with externally tunable interaction sites by playing with temperature or ionic strength [35].

Another method of interest for the preparation of CMs is the crystal templating strategy, which relies on the use of binary colloidal crystals (CCs) as templates and leads exclusively to AX_{12} CMs. Zhang and coworkers have applied this strategy to soft PNIPAM microgel submicron CAs [36]. In *fcc*- or *hcp*-like CCs prepared by sedimentation from a 40 : 1 mixture of PNIPAM microspheres with surface thiol groups and surface vinyl groups, the latter are statistically in close contact with 12 CAs bearing

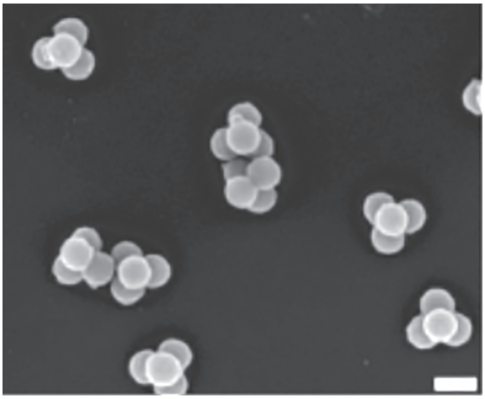

Figure 1.3 FESEM micrograph of tetrahedral CMs. Scale bar: 200 nm. Source: Wagner et al. [33] / with permission of American Chemical Society.

thiol groups. Under UV light irradiation, the thiol–ene reaction allows the covalent binding of the 13 microspheres, which are recovered as independent CMs after the destruction of the CCs. By-products with a higher number of microspheres have been found in the same batch but easily removed by density gradient centrifugation. The same strategy has been extended to AX_4, AX_5, and AX_6 CMs using vinyl-PNIPAM microspheres smaller than the thiol-PNIPAM ones in order to accommodate them in the interstitial sites of different close-packed lattices [37]. An enhanced crystal templating method has been investigated by Crocker and colleagues using PS microspheres coated with DNA strands (Figure 1.4) [38, 39]. They have demonstrated that interactions between these colloids can be reprogrammed using enzymes or reinforcing DNA strands to prepare CMs (AX_n with $n = 4, 6, 8, 10$, or 12). In the enzymatic approach, two populations of DNA-coated CAs are mixed, with a large excess of the larger ones, and forced into close-packed crystal structures via centrifugation at low ionic strength [38]. At higher ionic strength, sequence-specific enzymatic ligation selectively creates a covalent bond between colloids of different natures. A final

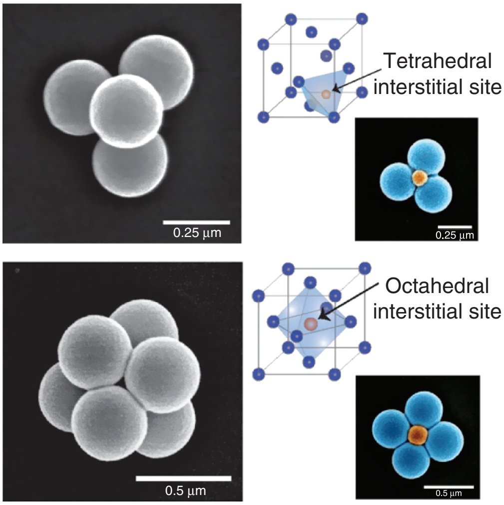

Figure 1.4 SEM images of tetrahedral and octahedral CMs produced using a colloidal crystal as a template (scale bars: 250 nm (top) and 500 nm (bottom). Source: McGinley et al. [38] / with permission of American Chemical Society.

washing step at low ionic strength destroys the crystals, thereby releasing the covalently bound CMs, which type depends on the size ratio between the two populations of colloids, i.e. the valence of the interstitial site occupied by the minority colloid.

According to a similar clustering strategy in 3D confinement, Tabeling and coworkers have reported a strategy to obtain CMs (X_n with $n = 3–6$) in microfluidic channels, thanks to the coupling of hydrodynamic dipolar interactions and depletion forces [40].

1.2.1.3 Clustering Assisted by Physical or Chemical Interactions

Clustering into AX_n CMs can also be quite simply achieved, thanks to the single sticky protrusion emerging from the surface of cross-linked polymer CAs when they are swollen with monomer and temperature is raised. In these conditions, the central CA is generated *in situ* and made of the merged protrusions. In this way, Kraft et al. have obtained CMs with AX_2–AX_9 morphologies from PS nanoparticles previously coated with vinyl acetate by delaying the polymerization of the protrusions for promoting coalescence upon collision before solidification upon polymerization [41, 42]. Interestingly, the swelling liquid can also be an apolar solvent allowing to reconfigure any CM into regular ones through minimization of the interfacial energy, thanks to a diffusion-limited aggregation process. The final morphology can be tuned by varying the surfactant concentration and swelling conditions, i.e. time, solvent nature, and ratio.

Close-packed planar CMs obtained under depletion conditions in a 2D cell have been achieved by Manoharan and coworkers [43]. Using this strategy it was possible to form CMs with AX_2, AX_3, AX_4, and AX_6 morphologies with high yield, simply by choosing the appropriate size ratio between the spherical building units [44]. They have shown that a yield as high as 90% is achievable for the fabrication of AX_4 morphologies in the absence of confinement just by adjusting the size ratio between two size-monodisperse populations of colloids to 2.41. This strategy seems efficient whatever the driving force used for assembly, e.g. DNA hybridization or electrostatic interactions.

Thanks to the pioneering works of Alivisatos', Mirkin's, and Sleiman's groups, DNA hybridization anchored at the surface of CAs provides a flexible tool to control in solution the formation of CMs and in particular from CAs of different sizes or chemical compositions [45–48]. DNA origamis provide a new opportunity for CM design. Gang and coworkers have shown that they can guide directional and specific interactions between isotropic gold nanoparticles to achieve X_6, planar c-X_4, and planar AX_4E_2 CMs in solution [49, 50]. Recently, Fan and coworkers developed a strategy to assemble gold nanoparticles into a large variety of CMs relying on a long single-stranded DNA chain containing polyadenine domains and encoding segments [51]. Once adsorbed at the surface of gold nanoparticles, thanks to the polyadenine domains, the DNA strands guide the assembly of satellite particles by hybridization of the encoding domains. They show fine control of the valence of the CMs as well as the size of each bound particles. Furthermore, chiral CMs have been realized by the introduction of three different DNA strands at chosen vertices of the origami frame combined with the use of three pairs of gold nanoparticles with

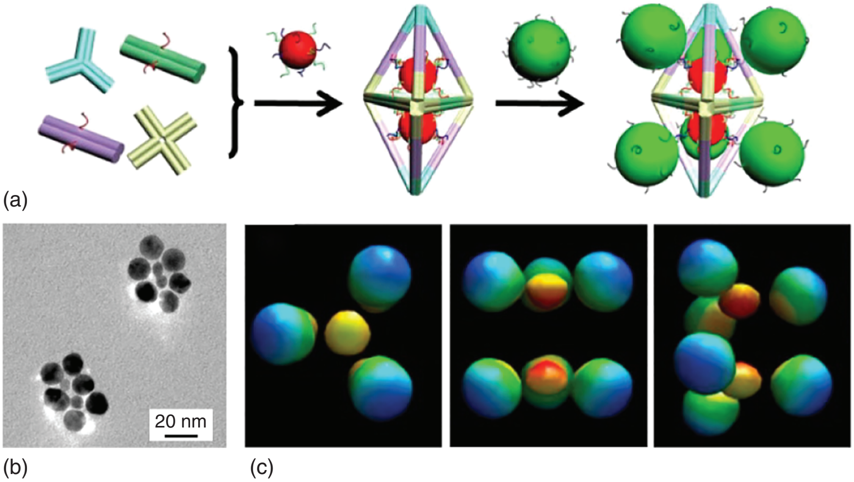

Figure 1.5 DNA frame guided-assembly of ethane-like CMs: (a) schematic representation of the assembly guided by a DNA cage, (b) corresponding TEM image, and (c) different views of the 3D reconstruction obtained by cryo-electron microscopy. Source: Li et al. [52] / with permission of American Chemical Society.

different sizes and complementary DNA shells [49]. Mao and coworkers have used DNA cages, i.e. smaller DNA constructs than origami that consist only of synthetic strands for trapping gold nanoparticles and guiding their assembly into AX_4 CMs with yields as high as 67%. This grants control over the geometry of AX_6 CM between octahedral and trigonal prismatic, as in SF_6 and $W(CH_3)_6$, respectively. Even more complex CMs such as dual-core ethane-like CMs frozen in an eclipsed conformation have been also achieved (Figure 1.5) [52].

To overcome the recurring problem of the too flexible DNA architectures that fail to maintain in the desired geometry the CMs made of bulky and heavy CAs, Chaikin and coworkers have designed a DNA origami belt that binds to the surface of 700-nm CAs and serves as guide for the later assembly of other DNA-coated CAs. This strategy not only yields X_4-derived chiral CMs but also allows controlling the dihedral angle between the particles (Figure 1.6) [53].

In an opposite approach, it may be relevant to fabricate CMs flexible at a will to mimic, to a certain extent, scissoring, rocking, twisting, or wagging vibrations of conventional molecules. The recent emergence of surface mobile DNA linkers provides new types of AX_n CMs ($n = 2$, 3, and 4) with flexible joints, where the satellite CAs remain free to move around the central one [54]. These central CAs forming these structures can be silica particles surrounded by a lipid-bilayer membrane into which DNA strands functionalized at their ends by cholesterol or stearyl moieties are anchored. As long as the lipid bilayers remain fluid, the DNA strands are free to move around the particles and so are the joints formed between CAs functionalized with complementary strands. These flexible CMs are physically stable but reorganize in permanence at high speed.

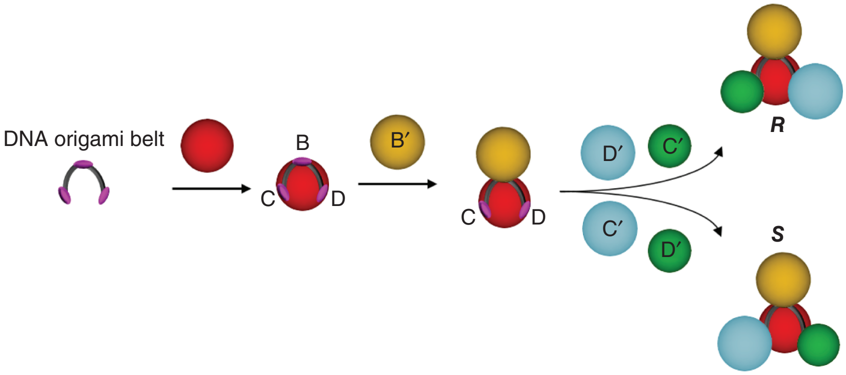

Figure 1.6 Schematic representation of the wrapping of a DNA origami belt around a first CA that guides the assembly of three other CAs into a chiral CM. Source: Modified from Ben Zion et al. [53].

1.2.2 Clustering of Patchy Particles

To mimic molecular geometry as best as possible, it is important to control not only the valence of the CAs but also the bond angles between them. We have shown in the previous section that this control can be exercised in an intrinsic way with more or less success by steric hindrance, electrostatic repulsions, or even the functionality of a DNA belt or origami. An increasingly explored alternative consists in programming this valence and directionality of interactions within CAs just as they are in conventional atoms, thanks to valence electrons. This is the concept of valence-endowed CAs, or patchy particles, where a patch is a surface discontinuity from the viewpoint of the chemistry or topography. They are promising colloidal building blocks not only for engineering CMs but also for open frameworks, if the number, relative location, size, and geometry of the patches can be precisely controlled [55]. The readers interested in a comprehensive description of the variety and synthesis pathways of patchy colloids is invited to refer to several recent reviews [17, 55, 56]. We focus here on their assembly capability to provide CMs. The patch-to-particle size ratio is one of the critical parameters to control the valence; roughly, the larger the patch, the higher the number of establishable bonds, especially as the patch number is low. Thus for getting CMs from patchy particles, there is mainly two routes: some X_n CMs may be more readily achieved from the clustering of one-patch particles, while AX_n ones can be generated from a central CA with the desired valence and the attachment of a single conventional CA to each of its patch.

1.2.2.1 Self-aggregation of One-Patch Particles, i.e. Janus Particles

As a subclass of patchy particles, Janus particles, named after the ancient roman god Janus [57], have extensively served as building blocks for CMs in the last few years, and the field has been recently reviewed [58–60]. Published examples concern Janus particles in the size range of 50-nm to 200-μm clustering into complex mixtures of CMs with aggregation numbers varying in the 2–20 range (Table 1.1).

Table 1.1 Representative examples of X_n CMs obtained from one-patch particles.

One-patch particles	Assembly driving force	Aggregation number	References
1-μm carboxylate-coated PS spheres then half-coated with gold treated with (11-mercaptoundecyl) ammonium chloride	Electrostatic attraction	2–12	[61]
1-μm carboxylate-modified PS spheres half-coated with gold treated with alkanethiol	Solvophobic effect helped with electrostatic screening	2–9	[62]
1-μm sulfate PS spheres half-coated with gold treated with alkanethiol	Hydrophobic attraction and electrostatic repulsion	2–7	[63]
4-μm snowman-like PS particles with smooth body and rough head	Roughness-controlled depletion attraction	2–12	[64]
2-μm organosilica particles with a partially embedded 1-μm hematite cube	Magnetostatic binding forces	2–3	[65]
3-μm gold half-coated silica spheres	At tipping points of thermally switched wetting	4–~20	[66]
4-μm iron oxide half-coated latex spheres	Lipid-induced capillary bridging	2–5	[67]
120-nm organosilica sphere with one 44-nm gold head	van der Waals force and electrostatic force	2–3	[68]
50-nm silica sphere with one 45-nm gold head coated with alkanethiols	Solvophobic effect	4–7	[69]
1-μm organosilica sphere with a PS patch (patch ratio of 0.13) that is functionalized with DNA having self-complementary sticky ends	DNA-mediated attraction varied by varying the temperature	2–4	[70]

The nature of the driving forces is generally physical, e.g. electrostatic, hydrophobic, or solvophobic interactions, roughness-controlled depletion, capillary bridging, or temperature-mediated DNA hybridization, meaning that bonding is quite weak or easily reversed. Therefore, the as-obtained CMs are fragile, making their purification difficult to impossible to succeed [71]. As far as we know, their strengthening by a chemical or physicochemical process has not yet been reported.

Nevertheless, three studies have been reported about the preparation of robust AX_n CMs. Bon and coworkers have synthesized asymmetric dumbbells made of a PS microsphere and a poly(*n*-butylacrylate) lobe and showed their ability to self-aggregate in aqueous media [72]. The desorption of the poly(vinylpyrrolidone)

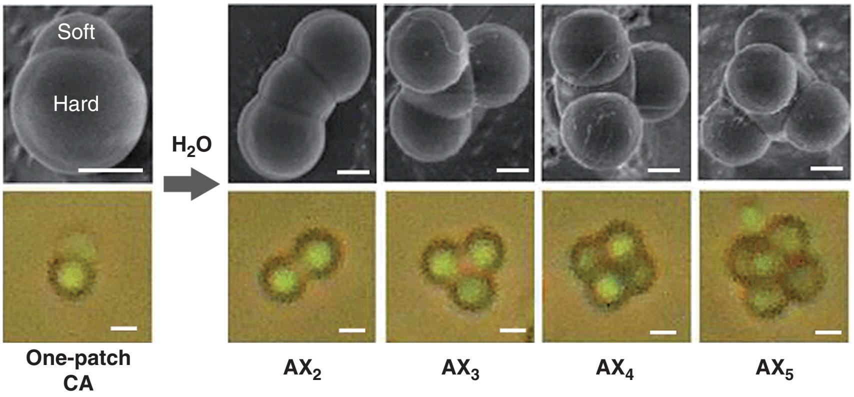

Figure 1.7 High resolution cryo-SEM (top row) and optical (bottom row) images of AX_n CMs in suspension obtained from polystyrene hard microspheres with a soft poly (*n*-butylacrylate) lobe (first column). Scale bars: 1 μm. Source: Skelhon et al. [72] / with permission of Royal Society of Chemistry.

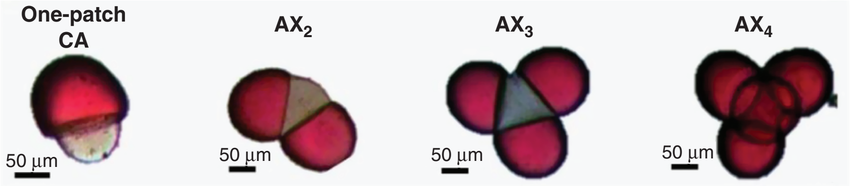

Figure 1.8 Optical microscopy images of CMs obtained from hydrophilic poly(ethylene glycol) diacrylate sphere with ethoxylated trimethylolpropane tri-acrylate lobe. Source: Ge et al. [73] / with permission of Wiley-VCH GmbH.

stabilizer from the particles trigger the assembly process through collision and merging of the soft poly(*n*-butylacrylate) lobes upon contact (Figure 1.7). Xu and colleagues have exploited the drying of aqueous Pickering emulsions made from 200-μm hydrophilic poly(ethylene glycol) diacrylate sphere with 160-μm ethoxylated trimethylolpropane tri-acrylate lobe prepared by microfluidics [73]. They have obtained quite regular CMs with aggregation numbers up to 8 (Figure 1.8). Lastly, we have recently reported the fabrication of CMs from silica/PS asymmetric dumbbell-like nanoparticles (Figure 1.9) [74]. In ethanol/DMF mixtures, the one-patch particles stick together by their PS lobe after swelling/plasticization by DMF. The as-obtained CMs present aggregation numbers from 2 to more than 6.

1.2.2.2 Stoichiometric Attachment of Colloidal Satellites Around Patchy Particles

Surface dimples or cavities on patchy particles are also named entropic patches because they can be exploited to attract and bind spheres with similar curvature radii through depletion forces [75]. Already exploited for the formation of CCs [76], the depletion technique has been extended to fabricate CMs from microparticles

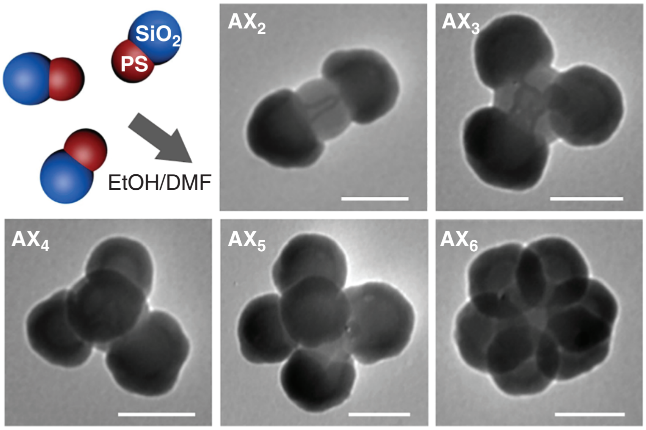

Figure 1.9 TEM images of CMs made of silica satellites and a PS central core obtained in ethanol/DMF mixture with a DMF fraction of 30 vol.%. Scale bars: 100 nm. Source: Li et al. [74] / with permission of Elsevier.

according to the lock-and-key principle proposed by Pine and coworkers [77–79]. They used silica microparticles with a well-defined number of cavities combined to conventional spheres, which diameter fits that of the dimples in the presence of poly(ethylene oxide) as depletant [79]. AX, AX_2, AX_3, AX_4, and AX_5 CMs were stoichiometrically achieved when increasing the valence of the patchy microspheres (Figure 1.10). This multivalent lock-and-key binding is reversible, i.e. disassembly occurring when the depletant concentration is lowered, and flexible as the spheres are rotating freely within the cavities. The authors have not reported a pathway to make these CMs permanent.

The same group has reported that DNA hybridization is another way to assemble one-patch particles around a multipatch one [80]. They have obtained new CMs from AX to AX_4 morphology (Figure 1.11). For high patch-to-particle size ratio, they have observed original CMs, which mimic ethylene molecules if the single oblong central particle is considered as embedding both carbon atoms. Stepwise self-assembly has been demonstrated with similar particles bearing two types of DNA strands, i.e. one type on the patches and another one on the remaining particle surface, taking advantage of the 10 °C difference between their melting temperature [81].

Lastly, our group has successfully implemented a covalent strategy and obtained silica CMs from dimpled nanoparticles by aminating PS macromolecules anchored at the bottom of the dimples [82]. Then, we have incubated them in DMF with silica nanospheres, which surface ester groups are activated in order to lock them within the dimples via amide bonds. TEM pictures show that the satellite particles occupy most of the dimples in a robust way, making centrifugation sorting possible (Figure 1.12). AX_2, AX_3, AX_4, AX_nE_m, and AX_nY_m CMs have been obtained from di-, tri-, and tetravalent particles, respectively, by playing with the stoichiometry and number of different types of silica satellites [83]. Chiral CMs have been also randomly observed by using four differently sized satellites [82].

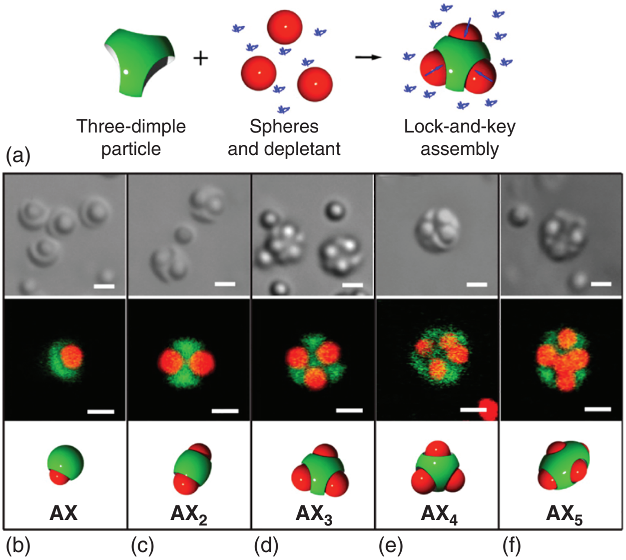

Figure 1.10 (a) Schematic illustration showing a three-patch particle with three assembled spheres using depletion interaction. The depletant (blue coil) causes osmotic pressure (arrows) between adjacent colloids, which is maximized when a sphere assembles into a cavity. (b–f) Bright field micrographs (top panel), confocal micrographs (middle panel), and cartoons (bottom panel) showing multivalent lock particles with (b) one, (c) two, (d) three, (e) four, and (f) five cavities binding to red fluorescent spheres stoichiometrically. Scale bars: 1 μm. Source: Wang et al. [79] / with permission of American Chemical Society.

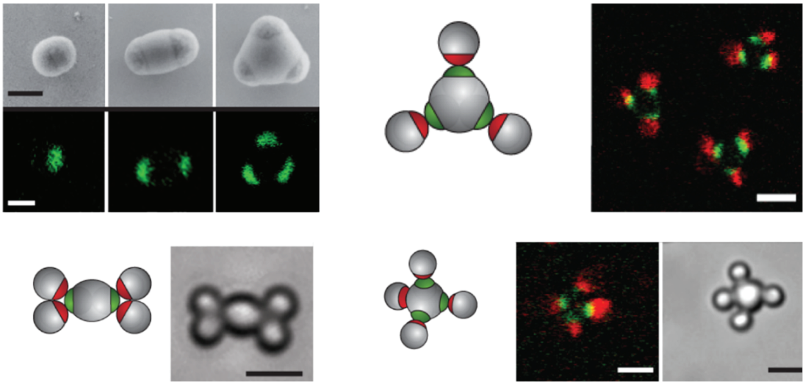

Figure 1.11 SEM and confocal fluorescent images of patchy particles used as CAs (scale bars: 500 nm) and bright-field confocal fluorescent images and schematics of CMs assembled from them through DNA hybridization (scale bars: 2 μm). Source: Wang et al. [80] / with permission of Springer Nature.

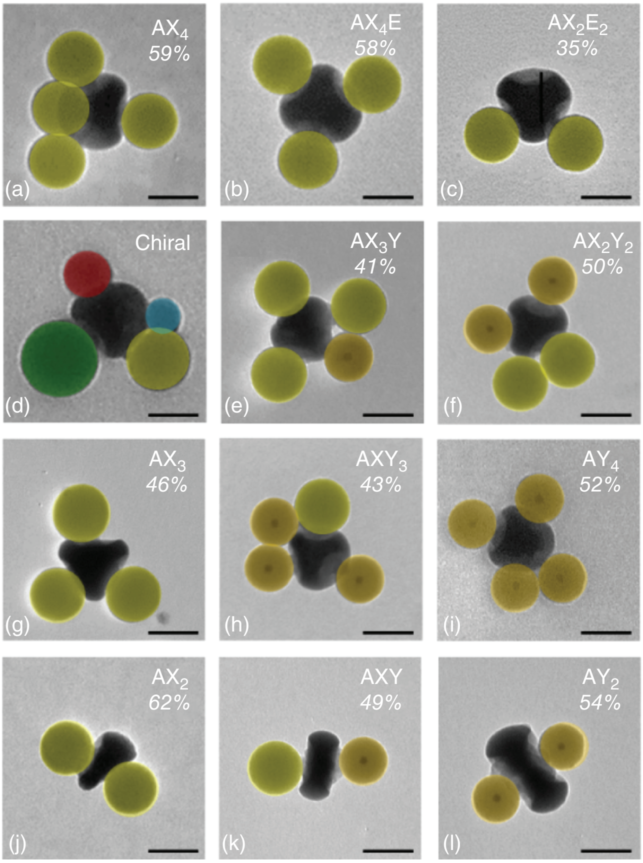

Figure 1.12 TEM images of silica CMs obtained by directional covalent bonding of patchy particles with four dimples (a–f; h–i), three dimples (g) and two dimples (j–l) and satellites of pure silica and different sizes labeled in yellow (100 nm), red (80 nm), blue (60 nm), and green (130 nm) or 90-nm silica satellites including a central gold dot (labeled in orange). Scale bars: 100 nm. The percentage value indicates the prevalence of the shown morphology knowing that exact stoichiometry of nanoparticles was used to obtain it. Scale bars: 100 nm. Source: Modified from Rouet et al. [82] and from Rouet et al. [83] / with permission of Wiley-VCH GmbH.

1.3 Colloidal Polymers: Mimicking Organic Macromolecules

The concept of using nano- or microparticles as “colloidal monomers” has received recent attention for the formation of 1D mesostructures, or “CPs.” [15, 84] These colloidal monomers form linear assemblies through directional, attractive, interparticle interactions, which are similar to covalent or supramolecular interactions in classical polymer science. However, in contrast to the high degree of structural control available in the synthesis of classical molecular polymers, methods to control fundamental structural features such as chain length or degree of polymerization

(DP), composition (copolymers), and architecture (linear, branched, etc.) are still being developed for CP systems. In this section, we provide a description of the different strategies that have been developed for the formation of CPs with examples chosen to evidence control of structure and composition. The use of patchy particles as monomers will be particularly emphasized given the growing number of studies on this subject in the recent years.

1.3.1 Dipole-Directed Formation of Colloidal Polymers

Dipole-directed colloidal polymerization refers to the formation of linear (or lightly branched) assemblies arising from coupling through space of charge or spin dipoles inherent to the inorganic cores of colloidal monomers. The colloidal polymerization is sensitive to changes in the composition and crystal phase of the material, where the attractive interparticle dipolar forces can be mitigated by ligand-induced repulsive interactions or increased temperature. Moreover, the architecture of the resulting CPs is dependent upon the balance between dipolar and van der Waals interactions between the constituent colloidal monomers.

1.3.1.1 Electric Dipoles

Tang et al. reported the spontaneous chaining of CdTe nanocrystals of different diameters stabilized by thioglycolic acid when they were allowed to age in the dark at room temperature for up to 48 hours [85]. The formation of chains of nanocrystals was attributed to the existence of strong dipole–dipole attraction, the energy of nanoparticle dipole attraction being estimated to 8.8 kJ/mole for a nanoparticle diameter of 3.4 nm and a center-to-center interdipolar separation of 4.4 nm. A face-to-face orientation of the CdTe nanocrystals in the CPs was later suggested by Monte Carlo simulations [86]. The same team also showed that the electric dipole induced formation of CPs of CdTe nanowires [87] and of "nano-centipedes," which resembled classical polymer brushes when silica-coated CdTe nanowires were used as monomers [88]. Yi et al. recently reported an elegant paradigm for the dipole-directed copolymerization of nanoparticles grafted with reactive block copolymers ligands into linear chains with periodic sequence [89]. Upon mixing in the presence of acid catalyst, the neutralization between colloidal monomers of two different types, A and B, generates electric dipole-like AB dimers that further assemble into alternating copolymers composed of tens of sequentially positioned monomers (Figure 1.13a).

1.3.1.2 Magnetic Dipoles

In the absence of any external magnetic field, strong interparticle interactions of the magnetic spin dipoles of the colloidal monomers induce the formation of linear chains. Thomas showed in a pioneering work that polymer-stabilized 20-nm cobalt nanoparticles spontaneously form chains [92]. Wei and coworkers synthesized dipolar cobalt nanoparticles that formed bracelets under zero-field conditions [93–96], and Puyn and coworkers developed the synthesis of dipolar cobalt nanoparticles functionalized with end-functionalized PS ligands, which spontaneously formed linear CPs [90, 97–99]. Interestingly, a nematic-type liquid crystalline assembly was

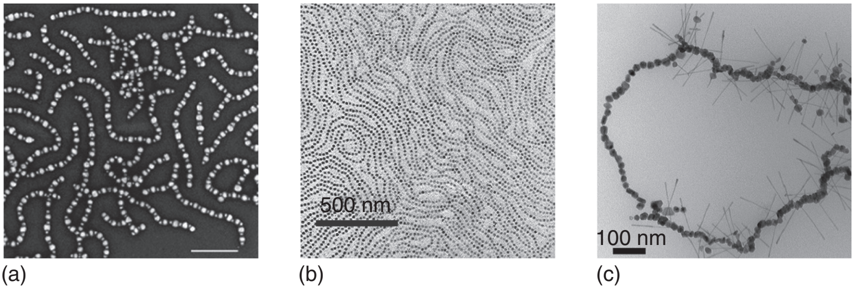

Figure 1.13 (a) SEM image of alternating copolymers made of inorganic nanoparticles of two different sizes (32 and 18 nm). Scale bar: 300 nm. Source: Yi et al. [89] / with permission of American Chemical Society. (b) TEM image of 1D assemblies of PS-coated cobalt nanoparticles. Source: Benkoski et al. [90] / with permission of American Chemical Society. (c) TEM image of cobalt-tipped semiconductor nanorods blended with free cobalt nanoparticles. Source: Hill et al. [91] / with permission of American Chemical Society

observed, where both strong north–south dipolar and weak antiferromagnetic coupling between nanoparticles dipoles was found, resulting in intermittent folding of the colloidal chains (Figure 1.13b). The same team prepared core–shell Au@Co nanoparticles by deposition of cobalt shells onto preformed gold seed nanoparticles [100]. These core–shell nanoparticles were capable to form linear assemblies due to spin dipolar interactions of the ferromagnetic cobalt shells. More complex polymer architectures were prepared from heterostructured monomers consisting in cobalt nanoparticles deposited onto semiconductor nanorods. Linear assemblies of these “matchstick” monomers were obtained due to dipolar magnetic coupling of the cobalt tips [91]. The preparation of block-type colloidal copolymers was also demonstrated by blending dipolar “bare” cobalt nanoparticles with cobalt-tipped semiconductor nanorods possessing cobalt nanoparticles of similar size and magnetization (Figure 1.13c).

1.3.2 Formation of Colloidal Polymers by Nanowelding

CPs composed of gold nanoparticles-tipped CdSe nanorods and consisted of several tens of monomers were fabricated through the destabilization of surface ligands on the gold domains by the addition of molecular iodine and the resulting coalescence of the exposed gold domains [101]. These coalesced gold tips were observed to be polycrystalline after nanowelding.

1.3.3 Formation of Colloidal Polymers Under Physical or Chemical Confinement

Physical confinement and attractive capillary forces have been successfully combined to organize few monodisperse spherical particles into a variety of colloidal chains with a predetermined geometric structure.

In order to fabricate chains of colloids ranging in size from several microns to a few nanometers, Xia et al. have used a fluidic cell with a lithographically patterned bottom surface, which is tilted at an angle and filled with a colloidal solution [102–104]. As the liquid dewets across the cell during template-assisted self-assembly (TASA), the capillary force dominates the assembly process if the particle density is chosen similar to that of the assembling liquid. Colloidal chains were also produced by using lithographically patterned surfaces to trap PS and silica beads into grooves. The length of the chain-type aggregates was determined by the longitudinal dimension of the templates, and the internal structure (linear versus zigzag) was defined by the relative ratio between lateral dimension of the templates and the diameter of the spherical colloids (Figure 1.14a–d). Next, the system is heated slightly above the glass transition temperature of the colloidal material to permanently bond together the spherical particles. Finally, the patterned substrate is dissolved to release the resulting colloidal chains. More complex heterogeneous linear chains were obtained by Wolf and coworkers, applying consecutive depositions with particles of different sizes or composition [30]. Lee et al. have developed an alternative method, called the polymorphic meniscus convergence (PMC) method in order to overcome the main limitation of TASA, which is the achievable linewidth of lithography needed to pattern the bottom surface of the fluidic cell, thereby limiting the technique to colloids with diameters of 50 nm and larger [105]. They used a flow cell made of a hydrophobic auxiliary substrate with templated features and a hydrophilic support arranged such that the colloidal dispersion can only infiltrate specific regions of the cell. As the colloidal dispersion dries in those regions, the menisci converge through the action of lateral capillary

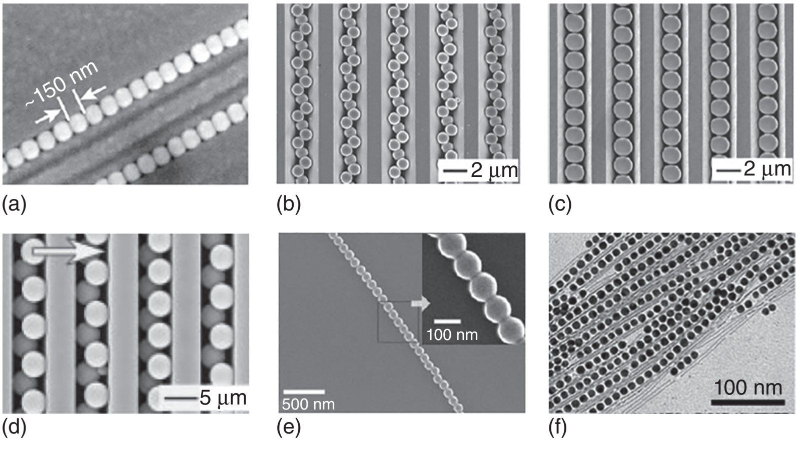

Figure 1.14 (a) SEM image of two linear chains of 150-nm PS beads. Source: Rycenga et al. [104] / with permission of Royal Society of Chemistry. (b–c) SEM images of two chainlike structures of PS beads assembled in 2D arrays of V-grooves. Source: Rycenga et al. [104] / with permission of Royal Society of Chemistry. (d) SEM image of double-layered zigzag chains of 4.3-μm PS beads assembled in an array of channels whose cross-sections were 5 μm in width and 5.5 μm in height. Source: Xia et al. [103] / with permission of Wiley-VCH GmbH. (e) SEM image of 1D chain of 97-nm particles. Source: Lee et al. [105] / with permission of Wiley-VCH GmbH. (f) TEM image of 1D chains of gold nanospheres driven by gold nanowires. Source: Sánchez-Iglesias et al. [106] / with permission of Wiley-VCH GmbH.

forces, and the colloidal particles align with the features of the auxiliary substrate (Figure 1.14e). The colloidal chains structure is determined by the height of the cell gap between the two surfaces as well as the width and depth of the template pattern. Nanoporous alumina membranes were also used by Sawitowski et al. to arrange gold nanoparticles in the form of chains [107]. Pre-synthesized nanoparticles were filled into the porous system by vacuum induction. By adding different amounts of gold colloid, the number as well as the length of the chains can be increased. Liz-Marzan and coworkers used highly anisotropic gold nanowires that drive the oriented assembly of spherical and rodlike gold nanoparticles into 1D chains (Figure 1.14f) [106].

A 2D template made of four different DNA tiles was employed to align gold nanoparticles into chains with nanometer-scale precision [108]. One of the tile types contained a long polyadenosine sequence designed to be unhybridized upon assembly of the 2D array, thereby allowing it to be used as an anchor for particle binding. Six nanometer gold nanoparticles were then functionalized with multiple strands of 3′-thiolated polythymine DNA, which allowed the NPs to bind to the polyadenosine sequences on the 2D DNA tile arrays. The same approach allowed the same research group to produce alternating parallel chains of 5-nm and 10-nm gold nanoparticles [109].

1.3.4 Field-Directed Formation of Colloidal Polymers

Applying external fields offers several advantages for the assembly of colloids. First, the external field can be turned on, off, or programmed with different patterns conveniently, which allows the annealing of assembled colloidal structures due to a temporary release of the colloids from the directing force. Second, the external field does not contaminate the sample, and, third, the strength, type, and effective length of field-induced interparticle can be tuned over a much wider range than that in self-assembly.

1.3.4.1 Electric Fields

Electric field is widely employed to direct the assembly of colloidal particles because most of them are responsive to electric field. Indeed, colloidal particles that have dielectric constant values that are different from that of the solvent acquire a dipole moment that is parallel to the external field. The use of electric fields in the directed assembly of spherical colloids has been nicely reviewed by Velev and Bhatt [110]. Electric field assembly can be performed in direct current (DC) and alternating current (AC) fields. Controllable parameters such as amplitude, frequency, wave shape/symmetry, and phase allow the precise adjustment of driving forces important during the assembly process. By applying an alternating electric field to latex spheres entrapped between planar electrodes, an alignment of the particles into chains due to the attractive interactions between the induced dipoles was observed after 2 s [111]. The chains are parallel to the direction of the applied field and thus are perpendicular to the gap between the two electrodes. Chaining of charged and sterically stabilized polymethyl methacrylate (PMMA) spheres in a density- and

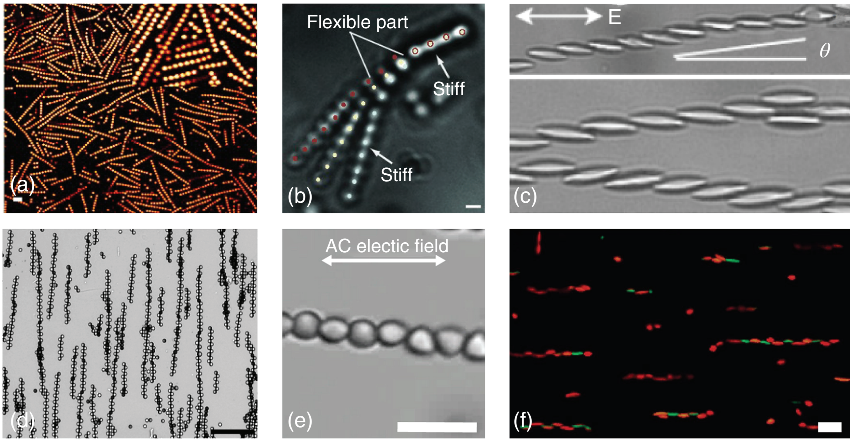

Figure 1.15 (a) Confocal micrographs of permanent PMMA chains in cyclohexyl bromide; the upper inset is a magnified view of the bead chains. Scale bar: 5 μm. (b) Color-coded overlay of optical micrographs of a triblock copolymer-like chain of PS beads taken at different times; the overlay was constructed by placing the rigid end in the same position and orientation. Scale bar: 2 μm. Source: Vutukuri et al. [114] / with permission of Wiley-VCH GmbH. (c) Optical micrographs of PS latex ellipsoids into chains orienting at an angle with respect to the field. Source: Singh et al. [115] / with permission of American Physical Society. (d) Optical micrographs of staggered chains formed from Janus particles in AC field of 56 V/cm at 40 kHz. Scale bar: 70 μm. Source: Gangwal et al. [116] / with permission of American Chemical Society. (e) Optical microscopy image of a chain of three-patch particles. Scale bar: 5 μm. Source: Song et al. [117] / with permission of American Chemical Society. (f) Confocal laser-scanning microscopy image of staggered chains of Janus ellipsoids on application of an AC electric field. Scale bar: 5 μm. Source: Shah et al. [118] / with permission of Springer Nature.

refractive-index-matched solvent mixture [112] and of PMMA particles in tetrahydrofuran [113] or cyclohexyl bromide (Figure 1.15a) [114] was also observed under AC electric field. In the latter case, the timescale for chain formation is on the order of a few seconds and the average chain length could be increased by increasing the applied field strength. The same approach was followed to make rigid chains consisting of PS or silica@PMMA core–shell particles. By mixing flexible and rigid chains together and by subjecting the mixture to the same protocol that was used in making the constituent bead chains, triblock copolymer-like chains were obtained (Figure 1.15b) [114].

AC electric fields have also been used to assemble anisotropic particles such as PS latex ellipsoids with aspect ratios 3.0, 4.3, and 7.6 into chains orienting at an angle with respect to the field [115]. This angle decreases as the ellipsoid aspect ratio increases (Figure 1.15c). Chains of asymmetric colloidal dimers have been created by inducing anisotropic interactions among them under AC electric field when the particle density is ~15% [119]. The 1D chains are uniquely formed by alternating association between dimers with opposite orientations. Such a pattern was theoretically attributed to an exquisite balance between electrostatic (primarily dipolar) and electrohydrodynamic interactions. Patchy metallodielectric particles have been extensively aligned under DC or AC electric fields because of the ease to directionally deposit a metallic cap on dielectric spheres [120, 121]. Janus particles prepared from silica microspheres with one hemisphere coated with metal, covered with a thin silica protective layer, have been subjected to perpendicular AC electric field, and chains were observed when the electric field frequency reached the megahertz range [122]. When Janus particles consisting of PS particles covered by a gold cap are exposed to an AC electric field at low frequencies (<10 kHz) and medium field strengths (40–100 V/cm), the formation of chains that resemble to those obtained from plain dielectric particles is observed, whereas staggered chains form when frequency is increased [116]. In the staggered chains (Figure 1.15d), the gold caps touch each other to minimize the electrostatic energy. An expansion of this work to patchy particles with two patches on opposite poles reveals how the particles assemble into regular, straight chains parallel to the electric field lines at frequencies lower than ~50 kHz, no distinguishable orientation of the patches being observed at such low frequencies [123]. At higher frequencies (> ~50 kHz) of the field, however, the two-pole microspheres form staggered chains and unanticipated diagonal chains oriented at ~45° to the field direction. Colloidal particles with two or three negatively charged patches fabricated by the cluster encapsulation method form CPs when polarized by an AC electric field [117]. Interestingly, the chains exhibit segments with a 2_1 screw axis symmetry due to a 180° rotation of successive particles along the chain, which creates favorable dipole–dipole interactions between polarized patches according to solid models (Figure 1.15e). Shah et al. showed that Janus ellipsoids that have been synthesized by the sequential deposition of 7.5 nm of chrome and 15 nm of gold on a monolayer of ellipsoidal particles assemble into staggered chains at high frequencies (Figure 1.15f) [118]. Chaining corresponds with a minimization of electrostatic energy, as the electric dipole moment of the Janus ellipsoids moves away from the ellipsoid's center of mass toward the extremities of the gold half of the particles. Shields et al. synthesized a wide range of anisotropic, patchy microparticles combining photolithography and metal deposition [124]. They showed that particles were attracted toward each other dielectrophoretically and they reoriented and aligned so that their edges were parallel and orthogonal to the field direction such that the particles organized into chains, usually with the metallic patch aligned with the field direction. It was also shown that composite dumbbells incorporating an asymmetrically placed titania sphere formed colloidal chains, in which they contacted their core—shell parts and oriented perpendicularly to a low-frequency (kHz) field, whereas they oriented parallel to a high-frequency (MHz) field [125].

1.3.4.2 Magnetic Fields

Colloids with magnetic properties in magnetic fields behave very similar to polarized particles in electric fields. Magnetic fields have also been extensively employed to direct the assembly of magnetic colloidal particles, with key factors that determine the final assembly equilibrium being the magnitude of magnetic interactions as well as the local particle concentration [126]. The strength of external magnetic fields directly determines both factors and enables full control of the assembly of particles into desired structures. Furst et al. created colloidal chains by applying a magnetic field to a suspension of paramagnetic PS spheres containing magnetite [127]. Chains were made permanent by covalent linking of the beads using glutaraldehyde. A similar strategy using streptavidin–biotin binding was employed by Biswal and Gast to produce flexible magnetoresponsive chains, which mechanical properties were studied [128]. Zhang et al. produced chains of 150-nm Fe_3O_4 particles under magnetic field [129]. The length of the chains increased with increasing field intensity, while the diameter of the particle in the chains remained nearly constant. The average length of the chains increased from 1.5 to 4 μm with the synthesizing field varying from 1000 to 3500 Oe. A convenient and flexible approach for the fabrication of colloidal chains exhibiting photonic properties was proposed by Yin and colleagues [130–132]. The colloidal monomers were Fe_3O_4 colloidal nanocrystal clusters, which were assembled into chains by applying a magnetic field. All the chains aligned along the field direction so that the dispersion diffracts light and shows brilliant colors. In response to the change of the strength of the external field, the periodicity of the chainlike structures alters. The diffraction wavelength is therefore responsive to external magnetic fields. After carefully optimizing the sizes of nanocrystal clusters, their diffraction wavelength or color can be effectively tuned within the visible light spectrum, from blue to green and to red. The color change occurs instantly upon the change in field strength. A similar study was reported by Hu et al. in which the Fe_3O_4 colloidal nanocrystal clusters were coated with a thin layer of silica and the chains were overcoated with an additional layer of silica to stabilize their structure (Figure 1.16a) [133]. Recently, Yellen and coworkers have chained superparamagnetic particles by the magneto-acoustic method, already described earlier [28]. At low particle concentration, they observed the formation of CPs when the tilt angle of the applied magnetic field was higher than 60°, whereas chaining occurs as soon as the tilt angle is $>0°$ for intermediate particle concentrations. Bannwarth et al. obtained homopolymers under magnetic field from monodisperse superparamagnetic PS nanoparticles [134]. The chain length can be tuned either by the concentration of the nanoparticles dispersion or by the growth time of the chains. When dispersions with higher polydispersity were used, a sequencing analogous to that known from polymer chemistry can be observed. Indeed, block- or statistical copolymer-like sequencing of nanoparticles with different sizes was observed depending on the assembly conditions. This is because a particle's dipole is proportional to its volume. At a given field strength, stronger dipolar forces between larger particles always assemble them first into linear chains. Chains made of smaller particles form later and attach to chains of larger particles as the field strength is further increased. If the field is ramped up instantaneously, such a sequential assembly will be suppressed, and the resulting chains exhibit statistically random sequences. It was also observed that the size ratio of two neighboring particles can be used to introduce junction points into the linear arrangement of the hybrid nanoparticles induced by the magnetic field, giving rise to branched polymer networks (Figure 1.16b). More precisely, the combination of a large particle with several small binding partners provides the basis for a junction. The larger the size ratio of two neighboring particles, the more small particles "fit" next to a large particle.

Anisotropic magnetic particles have also been used as precursors of CPs when exposed to magnetic fields. Lee and Liddell reported the synthesis of peanut-shaped hematite particles coated by thin layer of silica and their assembly to form kinked zigzag chains under a DC field [138]. Chaining was also observed when a magnetic field was applied to monodisperse hematite ellipsoids [139]. Zerrouki et al. have shown that silica particles with a magnetic cap self-assemble into chains under an external magnetic field by ordering alternatively up and down along the chain direction [135]. This specific ordering results from the capped particles that have a magnetic dipole interaction, which is maximized when the circular bases of the caps are parallel to each other, parallel to the field, and as close together as possible (Figure 1.16c). In the same paper, they reported that symmetric dumbbells made of two silica particles with a solid magnetic ring located around the contact point between the two silica spheres also formed chains in which they rotate by 90° relative to their neighbors along the chain and field direction. Sacanna et al. synthesized magnetic particles made of an organosilica polymer sphere with a single hematite micromagnet embedded and their arrangement into long linear structures when an external magnetic field is imposed [65].

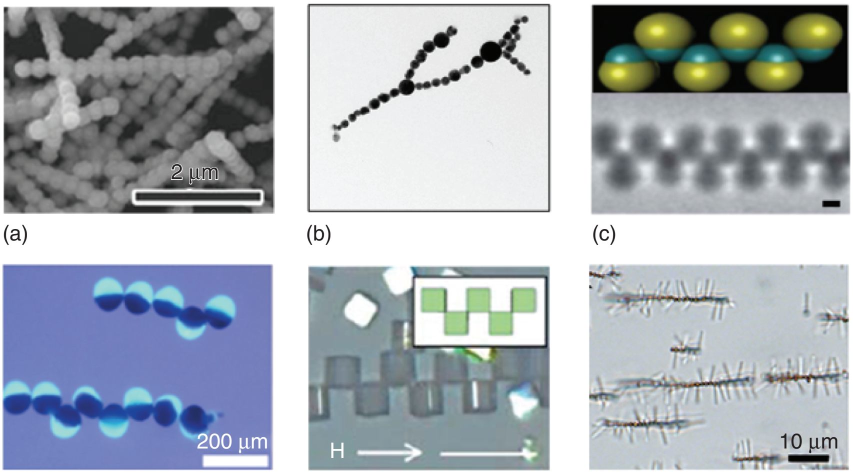

Figure 1.16 (a) SEM image of CPs made of Fe_3O_4 nanoparticles. Source: Hu et al. [133] / with permission of Wiley-VCH GmbH. (b) TEM image of a branched polymer network where the larger nanoparticles act as junction point. Source: Bannwarth et al. [134] / with permission of American Chemical Society (c) Optical microscope image and its corresponding schematic representation of chains of silica particles capped with a magnetic cap. Scale bar: 1 μm. Source: Zerrouki et al. [135] / with permission of Springer Nature. (d) Microscopic image of single pearl chains of Janus hydrogel microparticles under precessional magnetic field. Source: Yoshida et al. [136] / with permission of American Institute of Physics. (e) Optical micrograph of zigzagged chains of top-coated cubes. Scale bar: 25 μm. Source: Wyatt Shields Iv et al. [124] / with permission of Royal Society of Chemistry. (f) Optical microscopic image showing the directed assembly of Janus magnetic rods into chains under an external magnetic field. Source: Zhao et al. [137] / with permission of Royal Society of Chemistry.

The chaining behavior of magnetic Janus particles under an external magnetic field has also been extensively studied. Compartmental magnetic Janus spheres produced by phase separation approaches form staggered chains parallel to the field lines with the magnetic hemispheres pointing inward [140, 141], whereas the application of a precessional magnetic field to compartmental magnetic Janus hydrogel particles led to the formation of single or double pearl chains (Figure 1.16d) [136]. Staggered chains were also produced by applying a magnetic field to Janus particles prepared by partially coating one hemisphere of PS microspheres with a 34-nm layer of iron [124] or iron oxide [142]. When the thickness of the iron layer was smaller (8 nm), Janus particles form staggered or double chains in a magnetic field of 0.15 T, both oriented along the magnetic field direction. Recently Erbe and coworkers developed Janus magnetic particles prepared by coating a PS sphere with a multilayer stack of cobalt, palladium, and tantalum [143]. Under no applied field and guided by their long-range magnetic interaction, the particles assembled into a network of chains, connected by branching points. The authors showed that an applied oscillating magnetic field in plane or out of plane lead to the formation of chains with the amplitude of the field as a knob to tune the chain's conformation: staggered or linear. Shields et al. have fabricated microcubes and microcylinders in SU-8 coated with a thin layer of nickel [124]. With the application of a magnetic field parallel to the plane of a chamber containing an aqueous dispersion of top-coated microcubes, the authors observed the formation of zigzagged chains, whereas linear chains were fabricated when the particles were dispersed in ferrofluid due to the efficient formation of magnetic quadripoles resulting from the presence of the diamagnetic SU-8 component with respect to the ferrofluid magnetization (Figure 1.16e). Top-coated cylinders in water and in ferrofluid exhibited a similar behavior than top-coated cubes. Another interesting class of anisotropic magnetic precursors consists in magnetic silica rods. Yan et al. produced such objects by coating silica rods with a thin hemicylindrical magnetic layer of nickel [144]. When exposed to a magnetic field, the particles stack into kinked zigzag chains. Another synthetic approach based on the anisotropic growth of silica on the surface of Fe_3O_4 microspheres was developed by Zhao et al. to fabricate magnetic silica rods [137]. Under a DC magnetic field, the rods assemble into chains (Figure 1.16f).

1.3.5 Ligand-Directed Formation of Colloidal Polymers

The chemical interactions of surface ligands between neighboring particles have been widely used to dictate their 1D assembly into CPs and can be classified in several categories: electrostatic, covalent, or noncovalent interactions.

1.3.5.1 Electrostatic Interactions

Lin et al. reported the preparation of discrete chains, bifurcated and looped chains, or interconnected chain networks of negatively charged gold nanoparticles using a facile method based on the controlled replacement of citrate ions adsorbed onto the surface of the nanoparticles with covalently bound neutral mercaptoethyl alcohol molecules [145]. In so doing, electrostatic repulsion between the gold nanoparticles is progressively reduced and the stability of the electric dipole associated with charge separation on the nanoparticle surface is potentially enhanced by spatial partitioning of the mercaptoethyl alcohol molecules and citrate capping ligands. Many groups have also reported that colloidal chains formed during the addition of ethanol and other polar organic solvents to aqueous gold nanoparticle solutions [146–149]. In order to clarify the assembly mechanism of gold nanoparticles in such solvents, Yin and coworkers carried out systematic studies indicating that residual salt in conjunction with ethanol, instead of ethanol itself, induces the assembly of gold nanoparticles in ethanol [150]. It was in particular shown that the CP length increased with increasing salt concentration. Xia and coworkers induced the assembly of gold nanoparticles into chainlike structures with tunable lengths and interparticle separations by adding $HS(CH_2)_nCOOH$ ($n = 2$, 10, and 15) into a suspension of gold nanoparticles in a mixture of ethanol and water [151]. The number of gold nanoparticles in the chainlike assemblies could be altered by varying the concentration of the thiol, while the interparticle distance between gold nanoparticles in the chain could be adjusted by using thiols of different chain lengths. The formation of linear chains induced by the addition of salt into a suspension in DMF of gold nanoparticles capped with a monolayer of 2-naphtalenethiol was reported by Yang et al. [152]. To prevent the dissociation or the aggregation of the chains upon drying during the preparation of the substrate for SEM or TEM imaging, the 1D assemblies were encapsulated in shells of polystyrene-block-poly(acrylic acid) (Figures 1.17a–b). The authors proposed that the linear chain formation was kinetically controlled and that charge repulsion among gold nanoparticles was the key factor directing linear aggregation. Block copolymers consisting in segments of gold nanoparticles of different diameters were also fabricated, taking benefit on the strong dependence of the repulsive forces between nanoparticles on their respective sizes. Linear composite chains with configurations reminiscent of those of di- or triblock copolymers have also been prepared from pH-sensitive gold nanoparticles by blending chains of 25-nm and 36-nm nanoparticles and by decreasing the pH value from 3.0 to 2.5 [155].

1.3.5.2 Covalent Bonding

Stellacci and coworkers demonstrated the ability to position two individual molecules at opposite poles of a spherical gold nanoparticle and use these molecules to direct the formation of linear nanoparticle chains [156]. These bifunctionalized nanoparticles are created by first forming a mixed monolayer on the surface of nanoparticles consisting of 1-nonanethiol and 4-methylbenzenethiol. These two molecules were reported to form ordered rings of alternating phases on the surface of the nanoparticles, creating two diametrically opposed defect points on the particle surface. The small molecules at the defect points were then replaced by 1-mercaptoundecanoic acid activated by *N*-hydroxysuccinimide in order to induce the formation of a large number of linear chains, containing between 3 and 20 gold nanoparticles. The interparticle distances along the chains were changed by performing the synthesis with one of two divalent linking molecules of different lengths. The same group adopted a similar approach to form chains

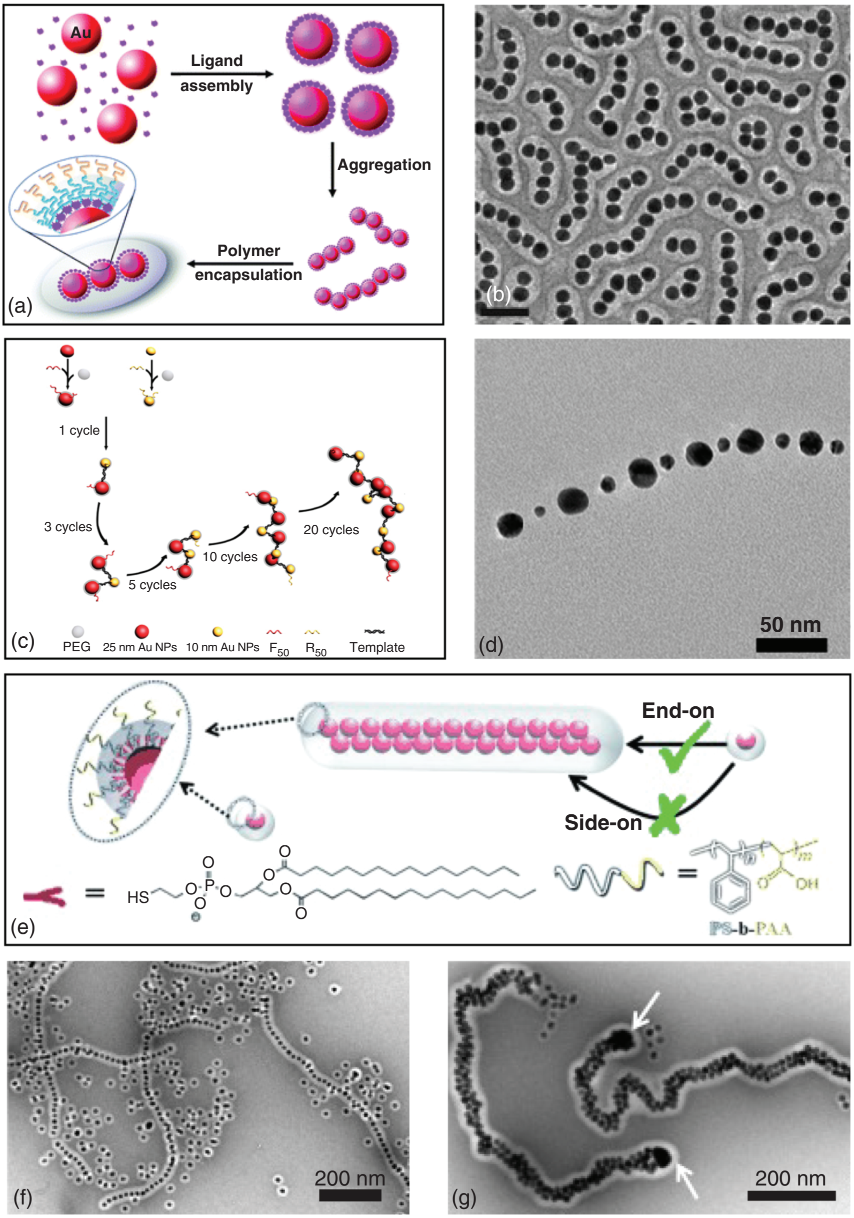

Figure 1.17 (a) Schematic illustration of the chains formation. (b) TEM image of chains of gold nanoparticles. Scale bar: 50 nm. Source: Yang et al. [152] / with permission from the Royal Society of Chemistry. (c) Schematic illustration of heterochains assembled based on PCR. (d) TEM image of heterochains of gold nanoparticles obtained by PCR. Source: Zhao et al. [153] / with permission of American Chemical Society. (e) Schematics illustrating the 1D assembly of gold nanoparticles encapsulated in Ps-b-PAA. (f) TEM image of single chains of AuNP@PSPAA. (g) TEM image of double-line chains of AuNP@PSPAA. The white arrows indicate the larger core–shell gold NPs used as seeds. Source: Wang et al. [154] / with permission of Wiley-VCH GmbH.

of superparamagnetic 13-nm iron oxide nanoparticles coated with a mixture of nonanoic acid and 4-phenylbutyric acid, which have “rippled” ligand shells with reactive polar point defects [157]. The chains showed ferromagnetic interactions between the nanoparticles that compose them, which raise the blocking temperature and hence the ferromagnetic phase of 40 K. α,ω-Dithiol molecules were also employed as linkers between gold nanorods [158] and CdSe nanorods possessing gold tips [159] to promote the formation of linear chains. In the latter system, the thiol groups bind strongly onto the Au tips, and the bifunctional molecules allow the preferential organization of CdSe nanorods as nanochains.

1.3.5.3 Noncovalent Attachment

Using Isotropically Capped Particles as Monomers Zhao et al. used polymerase chain reaction (PCR) to fabricate chains consisting of gold nanoparticles of different sizes, selectively capped with two oligonucleotide primers [153]. Alternating big and small chains were prepared by the DNA polymerization reaction directly on the surface of gold nanoparticles (Figures 1.17c–d). With an increasing number of PCR cycles, the number of nanoparticles in the assembled chains was found to increase from 2 up to 12. Taton and coworkers nicely showed that gold nanoparticles encapsulated within polystyrene-block-poly(acrylic acid) (PS-b-PAA) micelles assemble into regular 1D chains when they are exposed to solvent conditions that relax interfacial curvature in the micellar shell [160]. Nanoparticle chaining was induced by adding salt, acid, or cationic carbodiimide to the nanoparticles suspension. A similar approach was adopted by Chen and coworkers to fabricate linear assemblies (Figure 1.17e) [154]. The formation of “double-line chains” was observed through the addition of hydrochloric to a dispersion of the (PS-b-PAA) core–shell nanoparticles in a DMF/water (7 : 3, v/v) mixture at 70 °C and was attributed to the aggregation of the core–shell nanoparticles and subsequent reorganization of the polymer shells to form cylindrical micelles. When the DMF/water ratio was increased to 6 : 1, ultralong single chains were obtained (Figure 1.17f). In another set of experiments, the authors used larger core–shell gold nanoparticles of core–shell silver nanocubes as seeds to grow chains. The concentration of the seeds was too low that they could not aggregate upon destabilization under the acidic conditions. Upon addition of a large amount of small core–shell gold nanoparticles, “double-line chains” with large seeds at their end were obtained (Figure 1.17g). Choueiri et al. used gold nanospheres or silver nanocubes capped with PS ligands of different molecular weights as monomers and induced their assembly into chains by reducing the solvent quality for PS ligands [161]. Tiopronin-coated silver nanoparticles were also assembled under sonication into linear chains, which were held together by a combination of van der Waals forces, argentophilic interactions, and hydrogen bonding [162]. Periodically spaced and highly aligned 1D chains of hydrophilic polymer-grafted silver nanocubes were produced by introducing the metal blocks into a hydrophobic polymer matrix, which was annealed using thermal or solvent vapor treatment [163]. Chen and coworkers studied the self-assembly behavior of ultra-anisometric silver nanoplates capped with carboxylate-thiols [164]. Nanoplates behaved as bifunctional monomers and polymerized into chains upon the addition of sodium chloride. The assembly was found to proceed by a mechanism characteristic of molecular step-growth polymerization, since the number-average degree of polymerization grows linearly with time.

The precise control of the monomers' valence is crucial in order to self-assemble CPs. A valence 2 is indeed required to prevent branching or chain ends. Brujic and coworkers explored the use of emulsion droplets, decorated with DNA strands on the surface to assemble CPs [165]. Attached to the surface by lipids, the surface strands are still mobile. When two droplets bind through DNA hybridization, the authors showed that DNA strands were recruited at the contact points, forming a patch of high density while the rest of the surface was depleted of chains. A fine-tuning of the DNA coverage was shown to lead to a valence control when the amount of remaining DNA strands on the surface is too small to allow one more particle to bind. The same group showed a control of the monomer sequence by a careful design of the DNA sticky sequences [166]. They also recently showed that the polymers formed are dynamic and were models of freely joined polymers, at the micrometer scale [167].

Using Patchy Particles as Monomers The differential binding of ligands to the long sides or to the edges of gold nanorods was largely used to promote their assembly into CPs. Caswell et al. synthesized gold nanorods that were coated with cetyl trimethylammonium bromide (CTAB) and postulated that the molecular ligands preferentially bind along the long lateral facets of the nanorods [168]. They further bound biotin ligands onto the nanorod tips and induced chaining through the addition of streptavidin, since biotin binds tightly to streptavidin, with four biotins binding per protein. CPs containing at least ten nanorods were obtained. The same group reported a little bit later the formation of linear assemblies of CTAB-coated gold nanorods, nanospheres, and nanobipyramids, and attributed this assembly behavior to the lower stability of CTAB bilayers on nanoparticle surfaces with high curvature [169]. The regioselective binding of CTAB molecules along the lateral facets of gold nanorods and bipyramids was also exploited by Yan and coworkers to promote the formation of linear chains, branched chains, and necklace structures by the preferential attachment of glutathione or cysteine onto the terminal facets of the nanoparticles [170]. In a similar way, Kotov and colleagues have utilized the chromonic material disodium cromoglycate (DSCG) to end-to-end assemble negatively charged poly(acrylic acid) (PAA)-coated gold nanorods, since PAA was able to bind the positively charged CTAB-coated sides of the nanorods but not the tips, which were left to interact with DSCG via electrostatic or van der Waals forces [171]. By specifically grafting thiolated oligonucleotides on the tips of CTAB-coated gold nanorods, Pan et al. reported that metal blocks can be assembled preferentially in an end-to-end fashion upon the addition of oligonucleotides with complementary sequences [172]. Kumacheva and coworkers grafted thiol-terminated PS oligomers onto the tips of laterally CTAB-capped gold nanorods [173]. By adding water (20 wt%) (a bad solvent for PS) to a suspension of nanorods in dimethylformamide (a good solvent for both CTAB and PS), they reduced the solubility of PS, thereby triggering nanorod assembly in chains. The spacing between the adjacent nanorods in the chains was found to increase with increasing water content, due to a relocation of the PS tails from the long faces of the nanorods to the gaps between the metal blocks. The authors further investigated the evolution of the self-assembled chains, following the gradual change in the selectivity of solvent for the central CTAB-coated metal block and PS molecules [174]. They also performed a quantitative study of the assembly process in order to predict the chain topology and the kinetics of the chain growth [175]. The colloidal polymerization was shown to follow a step-growth polymerization model, the nanorods acting as multifunctional monomers and forming reversible, noncovalent bonds at specific bond angles. A similar conclusion was made when the polymerization was induced by the addition of salts, which was found to increase the assembly rate due to a salt-mediated reduction in the solubility of the PS ligands [176]. In order to provide insight into the polymerization kinetics, Au–Fe_3O_4 heterodimers were blended with PS-terminated gold nanorods in DMF/water mixtures, the heterodimers being utilized as "chain stopper." [177] The replacement of PS oligomers by poly(*N*-isopropylacrylamide) or random poly(styrene-*co*-isoprene) copolymers allowed the same group to photothermally trigger the assembly of gold nanorods in 1D structures [178] and covalently fix the bond angles in the CPs [179], respectively. Finally, the co-assembly of gold nanorods with different dimensions into random and block copolymers and of gold and palladium nanorods into random copolymers was also demonstrated [180] (Figure 1.18a).

Monodisperse and well-defined patchy micelles prepared by the solution self-assembly of amphiphilic block copolymers represent other very popular building blocks for the preparation of CPs. Pioneering work by Li et al. in 2004 [184] and by Cui et al. in 2007 [185] showed that patchy micelles prepared from triblock copolymers undergo further self-assembly to afford long linear chains, whereas branched assemblies could also be observed, probably due to polydispersity in size and shape of assembling micelle units [185]. By immersing assembled 1D structures into primary amine-coated gold nanoparticle aqueous suspension for several minutes, it was possible to regioselectively decorate the negatively charged zones of the CPs, giving rise to very interesting hybrid CPs [185]. Gröschel et al. synthesized a series of patchy micelles using triblock copolymers as precursors and induced their assembly in linear and branched chains by the introduction of a poor solvent for corona patches of the micelles [186]. Adding monovalent micelles in specific ratios to a solution of divalent micelles allowed the authors to control the length of the polymer chains, while multiblock co-assemblies were obtained by combining two types of divalent micelles (Figure 1.18b) [181]. In the same vein, Winnik and coworkers produced colloidal chains by placing cylindrical amphiphilic triblock micelles in nonsolvents for the central or terminal segments [187]. Sohn and coworkers fabricated CP chains by adding water in a DMF solution of two-patch micelles consisting in a central poly(4-vinyl-pyridine) core surrounded by two separated PS patches [188]. Random and block copolymer chains were also obtained by mixing two types of patchy micelles or two pre-polymerized chains, respectively. In remarkable later studies, the same group reported controlled branching of the CP chains by introducing well-defined trifunctional patchy micelles (Figure 1.18c) [182], the production of fluorescent chains from micelles containing fluorophores [189] and of chains containing gold or silver nanoparticles [190].

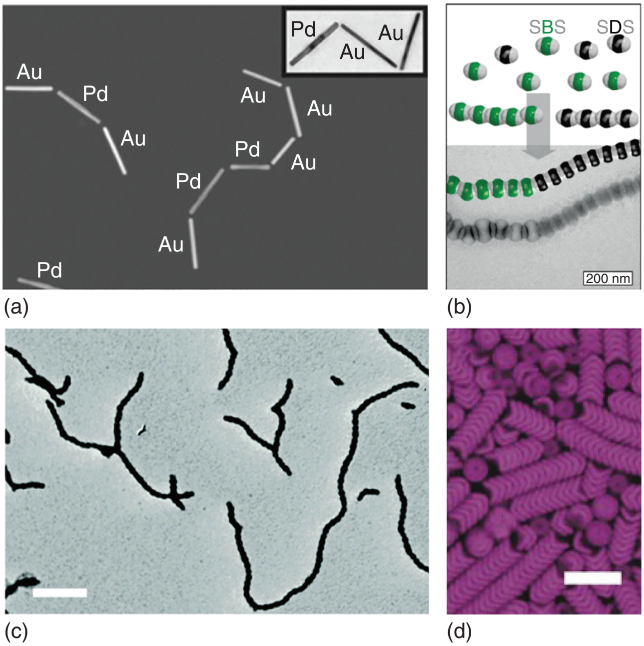

Figure 1.18 (a) STEM image of copolymers of palladium and gold nanorods. Scale bar: 500 nm. Source: Liu et al. [180] / with permission of Wiley-VCH GmbH. (b) Scheme and TEM image of the formation of colloidal copolymers by combining two types of divalent micelles. Source: Gröschel et al. [181] / with permission of Springer Nature. (c) TEM image of branched chains obtained by adding trifunctional micelles. Scale bar: 300 nm. Source: Lee et al. [182] / with permission of Royal Society of Chemistry. (d) SEM image of CPs made of cone-shaped particles. Scale bar: 10 μm. Source: Tigges and Walther [183] / with permission of Wiley-VCH GmbH.

Dielectric patchy particles were also employed as building units to fabricate CPs. Onoe and coworkers described sequential assembly of silicon microparts with two different binding sites in the form of 1D chains, thanks to hydrophobic and van der Walls interactions [191]. Depletion forces were also nicely exploited by Pine and coworkers [78] and by Walther and coworkers [183] to assemble colloidal particles with complementary geometrical forms into colloidal chains (Figure 1.18d). The co-assembly of cone-shaped particles with double-cone particles, which correspond to a homobifunctional monomer, nicely indicated a similar reactivity of both particles and a smooth "copolymerization." [183]

The formation of colloidal chains triggered by hydrogen bonding interaction [192] or biorecognition between complementary DNA strands [70] was also reported. In the latter case, the influence of the Janus balance of the chain structure was nicely investigated, and it was shown that dimer and trimer chains were obtained for intermediate and high patch ratio values (Figure 1.19a), respectively. Particles with two patches were also successfully employed as colloidal monomers. Combining depletion forces and triblock particles, Weck and coworkers recently demonstrated the selective formation of various chains (cross-chains, ladder, and tilted ladder

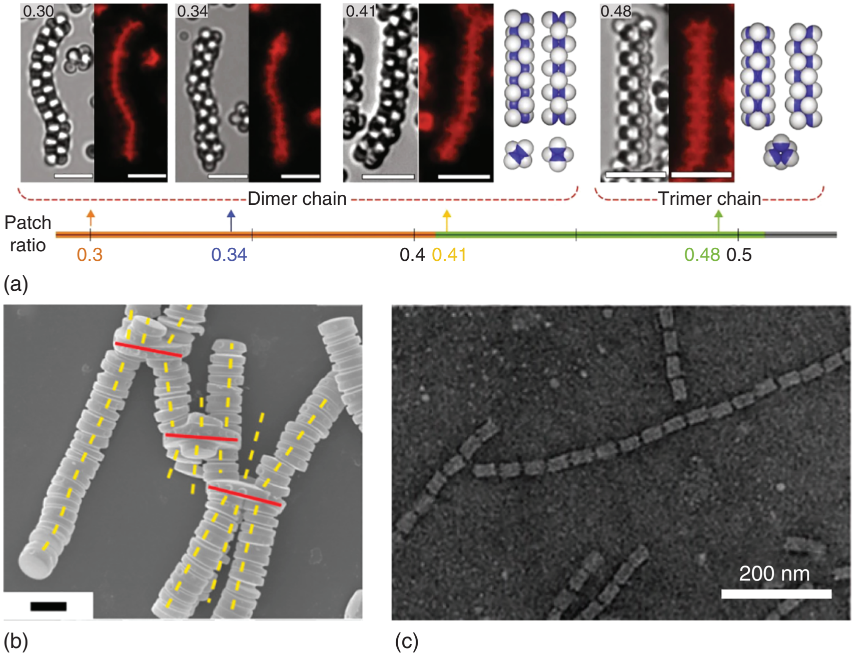

Figure 1.19 (a) Bright-field and fluorescent images of CPs made of DNA-coated Janus particles with patch ratios varying from 0.3 to 0.6. Scale bars: 10 μm. Source: Oh et al. [70] / with permission of Springer Nature. (b) SEM image of branch-like CPs resulted from the introduction of larger disks (represented by the red lines). Scale bar: 2 μm. Source: Zhao et al. [193] / with permission of American Chemical Society (c) TEM image showing polymeric chains of patchy DNA origami cuboids. Source: Tigges et al. [194] / with permission of American Chemical Society.

chains) of patchy particles [195]. They exploited the fact that the monomers formed of patches of PS with a core of polymerized 3-(trimethoxysilyl)propyl methacrylate (TPM) exhibit a directional and selective depletion interaction. In the presence of micelles of Pluronic F127 or Superonic F108, the particles bind selectively with a patch/patch or core/core interaction forming cross-chains or ladder chains depending on the overall shape of the monomer. The contrast of material giving rise to a hydrophobic contrast was also used by Shall and coworkers to assemble two-patch CAs into polymers using Casimir forces [196]. The monomers used were consist of hydrophobic patches of poly(methylmethacrylate) with an hydrophilic core of poly(methylmethacrylate-*co*-methacrylic acid). Once suspended in a mixture of heavy water and 3-methylpyridine (3MP) near the critical temperature, the particles interact through Casimir forces with temperature as the adjustment parameter, allowing the tuning of the bending stiffness between monomers as well as the interaction range. The authors showed that starting from a water-rich solvent gave rise to an attractive force between the hydrophilic cores of the particles forming a ladder-type polymer. On the contrary, a 3MP-rich solvent promoted the hydrophobic interaction between the patches, forming linear chains.

Liu and coworkers recently reported that capillary force can be used for directional 1D assembly of colloidal disks with two liquid patches [193]. By incorporating disks with larger diameters, which served as cross-linkers, the authors formed branch-like CPs (Figure 1.19b). We have produced colloidal chains from two-patch silica nanoparticles with PS chains at the bottom of their two cavities through reduction of the solvent quality for the PS chains [197]. We also showed that chain networks can be formed through the addition of three-patch nanoparticles, which play the role of branching points. Furthermore, block copolymers were also achieved by co-assembling preformed homopolymers composed of patchy NPs of different sizes or surface chemical groups. Pine and coworkers engineered PS-based particles with two patches functionalized with palladated pincer receptors and initiated the assembly by the addition of $AgBF_4$, which frees a coordination site for the pyridine-functionalized particles, thus allowing for the formation of linear and branched CPs [198]. The same research team took benefit of the inherent selectivity of host–guest assemblies to assemble particles with two patches functionalized with cucurbit[7]uril (CB[7]) into chains by the addition of diphenyl viologen (DPV) [199]. The resulting chains were sustained through the formation of CB[7]-DPV-CB[7] bridges and could be reversibly disassembled/reassembled by one-electron reduction/oxidation of the viologen. The group of New York University also fabricated alternating copolymers or homopolymers from two-patch particles site-selectively functionalized with complementary DNA strands [81, 200]. Programmable DNA hybridization was also employed to trigger the assembly of patchy, divalent DNA origami nanocuboids into chains (Figure 1.19c) [194]. Heating of the self-assembled chains led to disassembly into monomers, whereas subsequent cooling induced their reassembly.

1.4 Conclusion and Outlook

In this chapter, we have discussed the synthesis of CMs and CPs through the assembly of preformed particles. Indeed, a tremendous progress has been made in the synthesis of colloidal particles with a good size and shape selectivity over the last two decades, which are capable of exhibiting binding specificity via directional interactions and thus emerged as attractive building blocks [201]. Nevertheless, one can be sure that numerous advances in this field will be made in the near future, which would allow one to envision the preparation of a wider range of novel CMs and CPs, which will further open new avenues of research in the area of materials chemistry. For example, one can introduce orthogonal surface chemistries in designated patches [81] to guide the assembly of patchy particles into novel CMs. The orthogonal surface functionalization of colloidal monomers would also allow one to encode the required instructions to promote the folding of the resulting CPs into a 3D target structure [84, 202, 203]. Robust synthetic methods to control CPs architecture, regiochemistry, and composition also still need to be further developed, in order to afford useful, synergistic properties. For instance, the use of a colloidal analog of solid phase peptide synthesis is highly promising in order to control the sequence of colloidal monomers along the chains. Hence, we are convinced that the synthesis of CMs and CPs will remain a great source of inspiration for colloidal chemists, physical chemists, and physicists in a close future.

References

1 Grzybowski, B.A., Stone, H.A., and Whitesides, G.M. (2000). *Nature* 405: 1033.
2 Park, S., Lim, J.-H., Chung, S.-W., and Mirkin, C.A. (2004). *Science* 303: 348.
3 Pusey, P.N. and van Megen, W. (1986). *Nature* 320: 340.
4 Lu, P.J. and Weitz, D.A. (2013). *Annu. Rev. Condens. Matter Phys.* 4: 217.
5 Palberg, T. (2014). *J. Phys. Condens. Matter* 26: 333101.
6 van Blaaderen, A. (2006). *Nature* 439: 545.
7 Glotzer, S.C. and Solomon, M.J. (2007). *Nat. Mater.* 6: 557.
8 Sacanna, S. and Pine, D.J. (2011). *Curr. Opin. Colloid Interface Sci.* 16: 96.
9 van Blaaderen, A. (2003). *Science* 301: 470.
10 Plüisch, C.S. and Wittemann, A. (2013). *Macromol. Rapid Commun.* 34: 1798.
11 Morphew, D. and Chakrabarti, D. (2017). *Curr. Opin. Colloid Interface Sci.* 30: 70.
12 Elacqua, E., Zheng, X., Shillingford, C. et al. (2017). *Acc. Chem. Res.* 50: 2756.
13 Yu, B., Cong, H., Peng, Q. et al. (2018). *Adv. Colloid Interf. Sci.* 256: 126.
14 Duguet, E., Désert, A., Perro, A., and Ravaine, S. (2011). *Chem. Soc. Rev.* 40: 941.
15 Hill, L.J., Pinna, N., Char, K., and Pyun, J. (2015). *Prog. Polym. Sci.* 40: 85.
16 van Oostrum, P. (2017). *Design of Self-Assembling Materials* (ed. I. Coluzza), 91–106. Cham: Springer International Publishing.
17 Li, W., Palis, H., Mérindol, R. et al. (2020). *Chem. Soc. Rev.* 49: 1955.
18 Ning, H., Zhang, Y., Zhu, H. et al. (2018). *Micromachines* 9: 1.
19 Li, F., Josephson, D.P., and Stein, A. (2011). *Angew. Chem. Int. Ed.* 50: 360.
20 Rogers, W.B., Shih, W.M., and Manoharan, V.N. (2016). *Nat. Rev. Mater.* 1: 16008.
21 Scarfiello, R., Nobile, C., and Cozzoli, P.D. (2016). *Front. Mater.* 3: 1.
22 Plüisch, C.S. and Wittemann, A. (2016). Assembly of nanoparticles into "Colloidal Molecules": Toward complex and yet defined colloids with exciting perspectives. In: *Advances in Colloid Science* (eds. M.M. Rahman and A.M. Asiri), 237–264. InTech.
23 Löwen, H. (2018). *Europhys. Lett.* 121: 58001.
24 Wintzheimer, S., Granath, T., Oppmann, M. et al. (2018). *ACS Nano* 12: 5093.
25 Genix, A.-C. and Oberdisse, J. (2018). *Soft Matter* 14: 5161.
26 Ma, F., Wu, D.T., and Wu, N. (2013). *J. Am. Chem. Soc.* 135: 7839.
27 Demirörs, A.F., Pillai, P.P., Kowalczyk, B., and Grzybowski, B.A. (2013). *Nature* 503: 99.
28 Yang, Y., Pham, A.T., Cruz, D. et al. (2015). *Adv. Mater.* 27: 4725.
29 Wirth, C.L., De Volder, M., and Vermant, J. (2015). *Langmuir* 31: 1632.
30 Ni, S., Leemann, J., Buttinoni, I. et al. (2016). *Sci. Adv.* 2: e1501779.

31 Manoharan, V.N., Elsesser, M.T., and Pine, D.J. (2003). *Science* 301: 483.

32 Lauga, E. and Brenner, M.P. (2004). *Phys. Rev. Lett.* 93: 238301.

33 Wagner, C.S., Lu, Y., and Wittemann, A. (2008). *Langmuir* 24: 12126.

34 Schwarz, I., Fortini, A., Wagner, C.S. et al. (2011). *J. Chem. Phys.* 135: 244501.

35 Månsson, L.K., Immink, J.N., Mihut, A.M. et al. (2015). *Faraday Discuss.* 181: 49.

36 Yuan, Q., Gu, J., Zhao, Y. et al. (2016). *ACS Macro Lett.* 5: 565.

37 Yao, L., Li, Q., Guan, Y. et al. (2018). *ACS Macro Lett.* 7: 80.

38 McGinley, J.T., Wang, Y., Jenkins, I.C. et al. (2015). *ACS Nano* 9: 10817.

39 McGinley, J.T., Jenkins, I., Sinno, T., and Crocker, J.C. (2013). *Soft Matter* 9: 9119.

40 Shen, B., Ricouvier, J., Malloggi, F., and Tabeling, P. (2015). *Adv. Sci.* 3: 1.

41 Kraft, D.J., Vlug, W.S., van Kats, C.M. et al. (2009). *J. Am. Chem. Soc.* 131: 1182.

42 Meester, V., Verweij, R.W., van der Wel, C., and Kraft, D.J. (2016). *ACS Nano* 10: 4322.

43 Perry, R.W. and Manoharan, V.N. (2016). *Soft Matter* 12: 2868.

44 Schade, N.B., Holmes-Cerfon, M.C., Chen, E.R. et al. (2013). *Phys. Rev. Lett.* 110: 148303.

45 Alivisatos, A.P., Johnsson, K.P., Peng, X. et al. (1996). *Nature* 382: 609.

46 Aldaye, F.A. and Sleiman, H.F. (2007). *J. Am. Chem. Soc.* 129: 4130.

47 Mastroianni, A.J., Claridge, S.A., and Alivisatos, A.P. (2009). *J. Am. Chem. Soc.* 131: 8455.

48 Xu, X., Rosi, N.L., Wang, Y. et al. (2006). *J. Am. Chem. Soc.* 128: 9286.

49 Tian, Y., Wang, T., Liu, W. et al. (2015). *Nat. Nanotechnol.* 10: 637.

50 Liu, W., Halverson, J., Tian, Y. et al. (2016). *Nat. Chem.* 8: 867.

51 Yao, G., Li, J., Li, Q. et al. (2020). *Nat. Mater.* 19: 781.

52 Li, Y., Liu, Z., Yu, G. et al. (2015). *J. Am. Chem. Soc.* 137: 4320.

53 Ben Zion, M.Y., He, X., Maass, C.C. et al. (2017). *Science* 358: 633.

54 Chakraborty, I., Meester, V., van der Wel, C., and Kraft, D.J. Colloidal joints with designed motion range and tunable joint flexibility. *Nanoscale* https://doi.org/10.1039/C6NR08069C.

55 Ravaine, S. and Duguet, E. (2017). *Curr. Opin. Colloid Interface Sci.* 30: 45.

56 Pawar, A.B. and Kretzschmar, I. (2010). *Macromol. Rapid Commun.* 31: 150.

57 Perro, A., Reculusa, S., Ravaine, S. et al. (2005). *J. Mater. Chem.* 15: 3745.

58 Walther, A. and Müller, A.H.E. (2013). *Chem. Rev.* 113: 5194.

59 Zhang, J., Luijten, E., and Granick, S. (2015). *Annu. Rev. Phys. Chem.* 66: 581.

60 Zhang, J., Grzybowski, B.A., and Granick, S. (2017). *Langmuir* 33: 6964.

61 Hong, L., Cacciuto, A., Luijten, E., and Granick, S. (2006). *Nano Lett.* 6: 2510.

62 Hong, L., Cacciuto, A., Luijten, E., and Granick, S. (2008). *Langmuir* 24: 621.

63 Chen, Q., Whitmer, J.K., Jiang, S. et al. (2011). *Science* 331: 199.

64 Kraft, D.J., Ni, R., Smallenburg, F. et al. (2012). *Proc. Natl. Acad. Sci. U. S. A.* 109: 10787.

65 Sacanna, S., Rossi, L., and Pine, D.J. (2012). *J. Am. Chem. Soc.* 134: 6112.

66 Yu, C., Zhang, J., and Granick, S. (2014). *Angew. Chem. Int. Ed.* 53: 4364.

67 Bharti, B., Rutkowski, D., Han, K. et al. (2016). *J. Am. Chem. Soc.* 138: 14948.

68 Hu, H., Ji, F., Xu, Y. et al. (2016). *ACS Nano* 10: 7323.

69 Castro, N., Constantin, D., Davidson, P., and Abécassis, B. (2016). *Soft Matter* 12: 9666.

70 Oh, J.S., Lee, S., Glotzer, S.C. et al. (2019). *Nat. Commun.* 10: 3936.

71 Ben Zion, M.Y., Caba, Y., Sha, R. et al. (2020). *Soft Matter* 16: 4358.

72 Skelhon, T.S., Chen, Y., and Bon, S.A.F. (2014). *Soft Matter* 10: 7730.

73 Ge, X.-H., Geng, Y.-H., Chen, J., and Xu, J.-H. (2018). *ChemPhysChem* 19: 2009.

74 Li, W., Ravaine, S., and Duguet, E. (2020). *J. Colloid Interface Sci.* 560: 639.

75 Asakura, S. and Oosawa, F. (1954). *J. Chem. Phys.* 22: 1255.

76 Dinsmore, A.D., Yodh, A.G., and Pine, D.J. (1995). *Phys. Rev. E* 52: 4045.

77 Kim, S.H., Hollingsworth, A.D., Sacanna, S. et al. (2012). *J. Am. Chem. Soc.* 134: 16115.

78 Sacanna, S., Irvine, W.T.M., Chaikin, P.M., and Pine, D.J. (2010). *Nature* 464: 575.

79 Wang, Y., Wang, Y., Zheng, X. et al. (2014). *J. Am. Chem. Soc.* 136: 6866.

80 Wang, Y., Wang, Y., Breed, D.R. et al. (2012). *Nature* 491: 51.

81 Zheng, X., Wang, Y., Wang, Y. et al. (2016). *Chem. Mater.* 28: 3984.

82 Rouet, P.-E., Chomette, C., Duguet, E., and Ravaine, S. (2018). *Angew. Chem. Int. Ed.* 57: 15754.

83 Rouet, P.-E., Chomette, C., Adumeau, L. et al. (2018). *Beilstein J. Nanotechnol.* 9: 2989.

84 Cademartiri, L. and Bishop, K.J.M. (2015). *Nat. Mater.* 14: 2.

85 Tang, Z., Kotov, N.A., and Giersig, M. (2002). *Science* 297: 237.

86 Zhang, Z., Tang, Z., Kotov, N.A., and Glotzer, S.C. (2007). *Nano Lett.* 7: 1670.

87 Wu, L., Shi, C., Tian, L., and Zhu, J. (2008). *J. Phys. Chem. C* 112: 319.

88 Wang, Y., Tang, Z., Liang, X. et al. (2004). *Nano Lett.* 4: 225.

89 Yi, C., Yang, Y., and Nie, Z. (2019). *J. Am. Chem. Soc.* 141: 7917.

90 Benkoski, J.J., Bowles, S.E., Korth, B.D. et al. (2007). *J. Am. Chem. Soc.* 129: 6291.

91 Hill, L.J., Richey, N.E., Sung, Y. et al. (2014). *ACS Nano* 8: 3272.

92 Thomas, J.R. (1966). *J. Appl. Phys.* 37: 2914.

93 Tripp, S.L., Pusztay, S.V., Ribbe, A.E., and Wei, A. (2002). *J. Am. Chem. Soc.* 124: 7914.

94 Wei, A., Tripp, S.L., Liu, J. et al. (2009). *Supramol. Chem.* 21: 189.

95 Wei, A., Kasama, T., and Dunin-Borkowski, R.E. (2011). *J. Mater. Chem.* 21: 16686.

96 Wei, A. (2006). *Chem. Commun.*: 1581.

97 Keng, P.Y., Shim, I., Korth, B.D. et al. (2007). *ACS Nano* 1: 279.

98 Bowles, S.E., Wu, W., Kowalewski, T. et al. (2007). *J. Am. Chem. Soc.* 129: 8694.

99 Korth, B.D., Keng, P., Shim, I. et al. (2006). *J. Am. Chem. Soc.* 128: 6562.

100 Kim, B.Y., Shim, I.B., Araci, Z.O. et al. (2010). *J. Am. Chem. Soc.* 132: 3234.

101 Figuerola, A., Franchini, I.R., Fiore, A. et al. (2009). *Adv. Mater.* 21: 550.

102 Yin, Y., Lu, Y., Gates, B., and Xia, Y. (2001). *J. Am. Chem. Soc.* 123: 8718.

103 Xia, Y., Yin, Y., Lu, Y., and McLellan, J. (2003). *Adv. Funct. Mater.* 13: 907.

104 Rycenga, M., Camargo, P.H.C., and Xia, Y. (2009). *Soft Matter* 5: 1129.

105 Lee, S.W., Park, S.C., Lim, Y. et al. (2010). *Adv. Mater.* 22: 4172.

106 Sánchez-Iglesias, A., Grzelczak, M., Pérez-Juste, J., and Liz-Marzán, L.M. (2010). *Angew. Chem. Int. Ed.* 49: 9985.

107 Sawitowski, T., Miquel, Y., Heilmann, A., and Schmid, G. (2001). *Adv. Funct. Mater.* 11: 435.

108 Le, J.D., Pinto, Y., Seeman, N.C. et al. (2004). *Nano Lett.* 4: 2343.

109 Pinto, Y.Y., Le, J.D., Seeman, N.C. et al. (2005). *Nano Lett.* 5: 2399.

110 Velev, O.D. and Bhatt, K.H. (2006). *Soft Matter* 2: 738.

111 Lumsdon, S.O., Kaler, E.W., and Velev, O.D. (2004). *Langmuir* 20: 2108.

112 Yethiraj, A. and Van Blaaderen, A. (2003). *Nature* 421: 513.

113 Peng, B., van der Wee, E., Imhof, A., and van Blaaderen, A. (2012). *Langmuir* 28: 6776.

114 Vutukuri, H.R., Demirörs, A.F., Peng, B. et al. (2012). *Angew. Chem. Int. Ed.* 51: 11249.

115 Singh, J.P., Lele, P.P., Nettesheim, F. et al. (2009). *Phys. Rev. E.* 79: 050401.

116 Gangwal, S., Cayre, O.J., and Velev, O.D. (2008). *Langmuir* 24: 13312.

117 Song, P., Wang, Y., Wang, Y. et al. (2015). *J. Am. Chem. Soc.* 137: 3069.

118 Shah, A.A., Schultz, B., Zhang, W. et al. (2015). *Nat. Mater.* 14: 117.

119 Ma, F., Wang, S., Zhao, H. et al. (2014). *Soft Matter* 10: 8349.

120 Pawar, A.B. and Kretzschmar, I. (2008). *Langmuir* 24: 9057.

121 Zhang, G., Wang, D., and Möhwald, H. (2005). *Angew. Chem. Int. Ed.* 44: 7767.

122 Yan, J., Han, M., Zhang, J. et al. (2016). *Nat. Mater.* 15: 1095.

123 Gangwal, S., Pawar, A., Kretzschmar, I., and Velev, O.D. (2010). *Soft Matter* 6: 1413.

124 Wyatt Shields Iv, C., Zhu, S., Yang, Y. et al. (2013). *Soft Matter* 9: 9219.

125 Nagao, D., Sugimoto, M., Okada, A. et al. (2012). *Langmuir* 28: 6546.

126 Melle, S., Calderón, O.G., Rubio, M.A., and Fuller, G.G. (2002). *Int. J. Mod. Phys. B.* 16: 2293.

127 Furst, E.M., Suzuki, C., Fermigier, M., and Gast, A.P. (1998). *Langmuir* 14: 7334.

128 Biswal, S.L. and Gast, A.P. (2003). *Phys. Rev. E.* 68: 021402.

129 Zhang, Y., Sun, L., Fu, Y. et al. (2009). *J. Phys. Chem. C* 113: 8152.

130 Ge, J., Hu, Y., Zhang, T. et al. (2008). *Langmuir* 24: 3671.

131 Ge, J., Hu, Y., and Yin, Y. (2007). *Angew. Chem. Int. Ed.* 46: 7428.

132 Wang, M. and Yin, Y. (2016). *J. Am. Chem. Soc.* 138: 6315.

133 Hu, Y., He, L., and Yin, Y. (2011). *Angew. Chem. Int. Ed.* 50: 3747.

134 Bannwarth, M.B., Utech, S., Ebert, S. et al. (2015). *ACS Nano* 9: 2720.

135 Zerrouki, D., Baudry, J., Pine, D.J. et al. (2008). *Nature* 455: 380.

136 Yoshida, S., Takinoue, M., Iwase, E., and Onoe, H. (2016). *J. Appl. Phys.* 120: 084905.

137 Zhao, B., Zhou, H., Liu, C. et al. (2016). *New J. Chem.* 40: 6541.

138 Lee, S.H. and Liddell, C.M. (2009). *Small* 5: 1957.

139 Martinez-Pedrero, F., Cebers, A., and Tierno, P. (2016). *Phys. Rev. Appl.* 6: 034002.

140 Yuet, K.P., Hwang, D.K., Haghgooie, R., and Doyle, P.S. (2010). *Langmuir* 26: 4281.

141 Dyab, A.K.F., Ozmen, M., Ersoz, M., and Paunov, V.N. (2009). *J. Mater. Chem.* 19: 3475.

142 Ren, B., Ruditskiy, A., Song, J.H., and Kretzschmar, I. (2012). *Langmuir* 28: 1149.

143 Steinbach, G., Schreiber, M., Nissen, D. et al. (2019). *Phys. Rev. E* 100: 012608.

144 Yan, J., Chaudhary, K., Chul, B.S. et al. (2013). *Nat. Commun.* 4: 1516.

145 Lin, S., Li, M., Dujardin, E. et al. (2005). *Adv. Mater.* 17: 2553.

146 Liao, J.H., Chen, K.J., Xu, L.N. et al. (2003). *Appl. Phys. A Mater. Sci. Process.* 76: 541.

147 Zhang, H. and Wang, D. (2008). *Angew. Chem. Int. Ed.* 47: 3984.

148 Liao, J., Zhang, Y., Yu, W. et al. (2003). *Colloids Surf. A Physicochem. Eng. Asp.* 223: 177.

149 Zhang, H., Fung, K.-H., Hartmann, J. et al. (2008). *J. Phys. Chem. C* 112: 16830.

150 Han, X., Goebl, J., Lu, Z., and Yin, Y. (2011). *Langmuir* 27: 5282.

151 Cho, E.C., Choi, S.-W., Camargo, P.H.C., and Xia, Y. (2010). *Langmuir* 26: 10005.

152 Yang, M., Chen, G., Zhao, Y. et al. (2010). *Phys. Chem. Chem. Phys.* 12: 11850.

153 Zhao, Y., Xu, L., Liz-Marzán, L.M. et al. (2013). *J. Phys. Chem. Lett.* 4: 641.

154 Wang, H., Chen, L., Shen, X. et al. (2012). *Angew. Chem. Int. Ed.* 51: 8021.

155 Xia, H., Su, G., and Wang, D. (2013). *Angew. Chem. Int. Ed.* 52: 3726.

156 DeVries, G.A., Brunnbauer, M., Hu, Y. et al. (2007). *Science* 315: 358.

157 Nakata, K., Hu, Y., Uzun, O. et al. (2008). *Adv. Mater.* 20: 4294.

158 Shibu Joseph, S.T., Ipe, B.I., Pramod, P., and George, T.K. (2006). *J. Phys. Chem. B* 110: 150.

159 Mokari, T., Rothenberg, E., Popov, I. et al. (2004). *Science* 304: 1787.

160 Kang, Y., Erickson, K.J., and Taton, T.A. (2005). *J. Am. Chem. Soc.* 127: 13800.

161 Choueiri, R.M., Galati, E., Klinkova, A. et al. (2016). *Faraday Discuss.* 191: 189.

162 Shiers, M.J., Leech, R., Carmalt, C.J. et al. (2012). *Adv. Mater.* 24: 5227.

163 Gao, B., Arya, G., and Tao, A.R. (2012). *Nat. Nanotechnol.* 7: 433.

164 Luo, B., Smith, J.W., Wu, Z. et al. (2017). *ACS Nano* 11: 7626.

165 Feng, L., Pontani, L.-L., Dreyfus, R. et al. (2013). *Soft Matter* 9: 9816.

166 Zhang, Y., McMullen, A., Pontani, L.-L. et al. (2017). *Nat. Commun.* 8: 21.

167 McMullen, A., Holmes-Cerfon, M., Sciortino, F. et al. (2018). *Phys. Rev. Lett.* 121: 138002.

168 Caswell, K.K., Wilson, J.N., Bunz, U.H.F., and Murphy, C.J. (2003). *J. Am. Chem. Soc.* 125: 13914.

169 Sau, T.K. and Murphy, C.J. (2005). *Langmuir* 21: 2923.

170 Zhang, S., Kou, X., Yang, Z. et al. (2007). *Chem. Commun.*: 1816.

171 Park, H.S., Agarwal, A., Kotov, N.A., and Lavrentovich, O.D. (2008). *Langmuir* 24: 13833.

172 Pan, B., Ao, L., Gao, F. et al. (2005). *Nanotechnology* 16: 1776.

173 Nie, Z., Fava, D., Kumacheva, E. et al. (2007). *Nat. Mater.* 6: 609.

174 Fava, D., Nie, Z., Winnik, M.A., and Kumacheva, E. (2008). *Adv. Mater.* 20: 4318.

175 Liu, K., Nie, Z., Zhao, N. et al. (2010). *Science* 329: 197.

176 Liu, K., Resetco, C., and Kumacheva, E. (2012). *Nanoscale* 4: 6574.

177 Klinkova, A., Therien-Aubin, H., Choueiri, R.M. et al. (2013). *Proc. Natl. Acad. Sci.* 110: 18775.

178 Fava, D., Winnik, M.A., and Kumacheva, E. (2009). *Chem. Commun.*: 2571.

179 Lukach, A., Liu, K., Therien-Aubin, H., and Kumacheva, E. (2012). *J. Am. Chem. Soc.* 134: 18853.

180 Liu, K., Lukach, A., Sugikawa, K. et al. (2014). *Angew. Chem. Int. Ed.* 53: 2648.

181 Gröschel, A.H., Walther, A., Löbling, T.I. et al. (2013). *Nature* 503: 247.

182 Lee, S., Jang, S., Kim, K. et al. (2016). *Chem. Commun.* 52: 9430.

183 Tigges, T. and Walther, A. (2016). *Angew. Chem. Int. Ed.* 55: 11261.

184 Li, Z., Kesselman, E., Talmon, Y. et al. (2004). *Science* 306: 98.

185 Cui, H., Chen, Z., Zhong, S. et al. (2007). *Science* 317: 647.

186 Gröschel, A.H., Schacher, F.H., Schmalz, H. et al. (2012). *Nat. Commun.* 3: 710.

187 Qiu, H., Hudson, Z.M., Winnik, M.A., and Manners, I. (2015). *Science* 347: 1329.

188 Kim, J.-H., Kwon, W.J., and Sohn, B.-H. (2015). *Chem. Commun.* 51: 3324.

189 Kim, K., Jang, S., Jeon, J. et al. (2018). *Langmuir* 34: 4634.

190 Jang, S., Kim, K., Jeon, J. et al. (2017). *Soft Matter* 13: 6756.

191 Onoe, H., Matsumoto, K., and Shimoyama, I. (2007). *Small* 3: 1383.

192 Onishi, S., Tokuda, M., Suzuki, T., and Minami, H. (2015). *Langmuir* 31: 674.

193 Zhao, S., Wu, Y., Lu, W., and Liu, B. (2019). *ACS Macro Lett.* 8: 363.

194 Tigges, T., Heuser, T., Tiwari, R., and Walther, A. (2016). *Nano Lett.* 16: 7870.

195 Liu, M., Zheng, X., Grebe, V. et al. (2020). *Nat. Mater.* 19: 1354–1361.

196 Nguyen, T.A., Newton, A., Veen, S.J. et al. (2017). *Adv. Mater.* 29: 1700819.

197 Li, W., Liu, B., Hubert, C. et al. (2020). *Nano Res.* https://doi.org/10.1007/s12274.

198 Wang, Y., Hollingsworth, A.D., Yang, S.K. et al. (2013). *J. Am. Chem. Soc.* 135: 14064.

199 Benyettou, F., Zheng, X., Elacqua, E. et al. (2016). *Langmuir* 32: 7144.

200 Wang, Y., Wang, Y., Breed, D.R. et al. (2012). *Nature* 490: 51.

201 He, M., Gales, J.P., Ducrot, É. et al. (2020). *Nature* 585: 524.

202 Coluzza, I., van Oostrum, P.D.J., Capone, B. et al. (2013). *Phys. Rev. Lett.* 110: 075501.

203 Coluzza, I., van Oostrum, P.D.J., Capone, B. et al. (2013). *Soft Matter* 9: 938.